

The Final Report

Title: Ultra-Sensitive Biological Detection via Nanoparticle-Based Magnetically Amplified Surface Plasmon Resonance (Mag-SPR) Techniques

Principal Investigator:

Prof. Jinwoo Cheon (Yonsei University.)

Telephone: +82-2-2123-5631

E-mail: kenneth.jcheon@yonsei.ac.kr

Contract Number: FA4869-07-1-4069

AOARD Reference Number: AOARD-074069

AOARD Program Manager: Sang-ho Byun

Period of Performance: 1 year

Submission Date: 8 Oct. 2008

Report Documentation Page

Form Approved
OMB No. 0704-0188

Public reporting burden for the collection of information is estimated to average 1 hour per response, including the time for reviewing instructions, searching existing data sources, gathering and maintaining the data needed, and completing and reviewing the collection of information. Send comments regarding this burden estimate or any other aspect of this collection of information, including suggestions for reducing this burden, to Washington Headquarters Services, Directorate for Information Operations and Reports, 1215 Jefferson Davis Highway, Suite 1204, Arlington VA 22202-4302. Respondents should be aware that notwithstanding any other provision of law, no person shall be subject to a penalty for failing to comply with a collection of information if it does not display a currently valid OMB control number.

1. REPORT DATE 08 OCT 2008		2. REPORT TYPE Final		3. DATES COVERED 15-06-2007 to 14-06-2008	
4. TITLE AND SUBTITLE Nanoscale and Information Systems with Biological Implications				5a. CONTRACT NUMBER FA48690714069	
				5b. GRANT NUMBER	
				5c. PROGRAM ELEMENT NUMBER	
6. AUTHOR(S) Jinwoo Cheon; Donghoon Choi; Kunhong Lee; Jong Kim				5d. PROJECT NUMBER	
				5e. TASK NUMBER	
				5f. WORK UNIT NUMBER	
7. PERFORMING ORGANIZATION NAME(S) AND ADDRESS(ES) Korea Foundation for International Cooperation of Science & Technology, 275-7 Yangjae Dong, Seocho Gu, Seoul, South Korea, NA, NA				8. PERFORMING ORGANIZATION REPORT NUMBER N/A	
9. SPONSORING/MONITORING AGENCY NAME(S) AND ADDRESS(ES) AOARD, UNIT 45002, APO, AP, 96337-5002				10. SPONSOR/MONITOR'S ACRONYM(S) AOARD	
				11. SPONSOR/MONITOR'S REPORT NUMBER(S) AOARD-074069	
12. DISTRIBUTION/AVAILABILITY STATEMENT Approved for public release; distribution unlimited					
13. SUPPLEMENTARY NOTES					
14. ABSTRACT The report contains final reports from four separate projects co-funded by AFOSR/AOARD and Korean MEST. The four projects were (1) Ultra-Sensitive Biological Detection via Nanoparticle-Based Magnetically Amplified Surface Plasmon Resonance (Mag-SPR) Techniques; (2) Electronic, Photonic and Magnetic Properties of Natural and Modified DNA Complexes with Heavy Metals Ions; (3) Hierarchical Carbon Fiber Composites; and (4) Distributed Detection of Attacks/Intrusions and Prevention of Resource-Starvation Attacks in Mobile Ad Hoc Networks.					
15. SUBJECT TERMS					
16. SECURITY CLASSIFICATION OF:			17. LIMITATION OF ABSTRACT Same as Report (SAR)	18. NUMBER OF PAGES 55	19a. NAME OF RESPONSIBLE PERSON
a. REPORT unclassified	b. ABSTRACT unclassified	c. THIS PAGE unclassified			

1st Year Result Report

Ultra-Sensitive Biological Detection via Nanoparticle-Based Magnetically Amplified Surface Plasmon Resonance (Mag-SPR) Techniques

(자성 증폭 나노 입자를 이용한 초고감도 SPR 생체 진단기술 개발)

P.I.s: Profs. Jinwoo Cheon (Yonsei U.) & A. Paul Alivisatos (U. of California, Berkeley)

Research Goal: The ultimate goal of this project is to establish a fast, ultra-sensitive, and high-performance Mag-SPR nano-bio sensing technique by using integrated nanoparticles.

Research Purpose of Phase I: Fabrication of Mag-SPR probes and their feasibility test

- Synthesis of Mag-SPR probes
- Design & establishment of Mag-SPR imaging instrument

Research Contents

1. Fabrication of Mag-SPR probes (Korea):

- During the last research period (2007. 04. ~ 2008. 03.), we have tried to synthesize multi-component nanoparticles which contain both magnetic & metallic components with enhanced magnetism and plasmonic properties, respectively.

- We selected Mn-doped Magnetism-Engineered Iron Oxide (Mn-MEIO, MnFe_2O_4) nanoparticles with high magnetism and crystallinity as the magnetic core and synthesized by a high temperature nonhydrolytic organometallic precursor decomposition route (Cheon *et al*, *Nat. Med.* **2007**, *13*, 95). Obtained Mn-MEIO nanoparticles possess 15 nm size with high monodispersity ($\sigma \approx 7\%$) (Figure 1a) and enhanced magnetic properties (125 emu/g (Mn+Fe)) (Figure 1b-c).

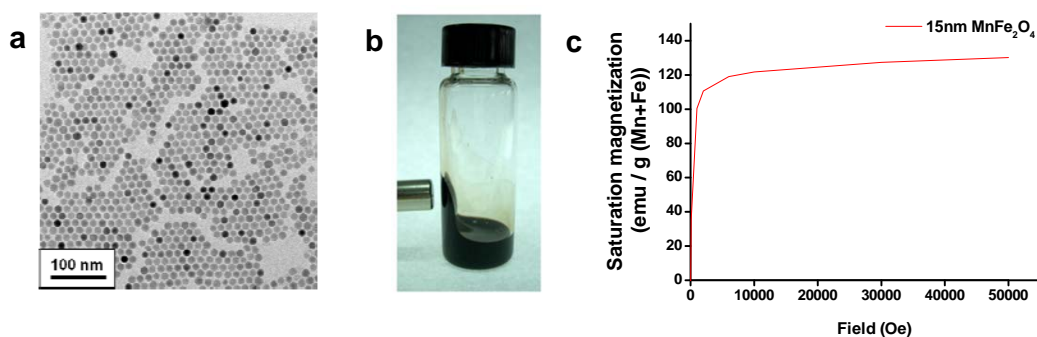


Figure 1. Transmission electron microscope (TEM) image and saturation magnetization value of Mn-MEIO (a) 15nm Mn-MEIO, (b) magnetic properties of Mn-MEIO dispersed in hydrophobic solvent, and (c) saturation magnetization values of 15 nm Mn-MEIO.

- Then, these Mn-MEIO nanoparticles were coated with dielectric SiO₂ via Stober method and subsequently coated with gold shells with high plasmonic properties and excellent bio-compatibility. Figures 2b and 2c show transmission electron microscopic images of Mn-MEIO@SiO₂ and Mn-MEIO@SiO₂@Au nanoparticles, respectively. Obtained Mn-MEIO@SiO₂@Au nanoparticles are ~ 70 nm in size with high monodispersity where the thickness of SiO₂ and Au shells are ~ 20 nm and ~ 9 nm, respectively. Our Mn-MEIO@SiO₂@Au nanoparticles show strong plasmonic peak around 620 nm.

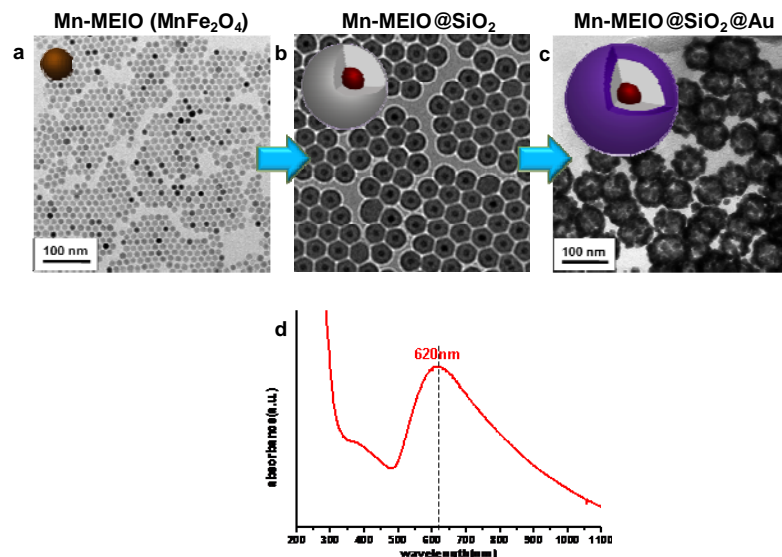


Figure 2. Transmission electron microscope image of (a) Mn-MEIO, (b) Mn-MEIO@SiO₂, and (c) Mn-MEIO@SiO₂@Au nanoparticles and (d) UV/Vis absorption spectra of Mn-MEIO@SiO₂@Au nanoparticles.

2. Design & establishment of Mag-SPR imaging instrument (US) and dark-field scattering imaging of nanoparticles in cells

- During last research period (2007. 04. ~ 2008. 03.), we have set up a dark field scattering microscope attached with CCD cameras (Andor iXon Camera), which enables ultra-fast (>10 kHz) dynamic Mag-SPR imaging of nanoparticle probes. Figure 3a shows the instrumental set up of the microscope.

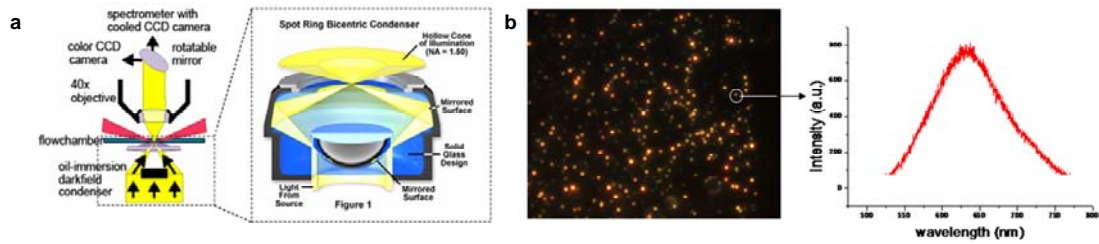


Figure 3. (a) Schematic of our dark field microscope, (b) Mag-SPR imaging of nanoparticle probes, and (c) absorption spectrum of single nanoparticle probe.

- We have successfully imaged single Mag-SPR nanoprobe through our dark-field microscopy (Figure 3b). This means that single-particle SPR imaging instruments was perfectly set up in UC Berkeley.

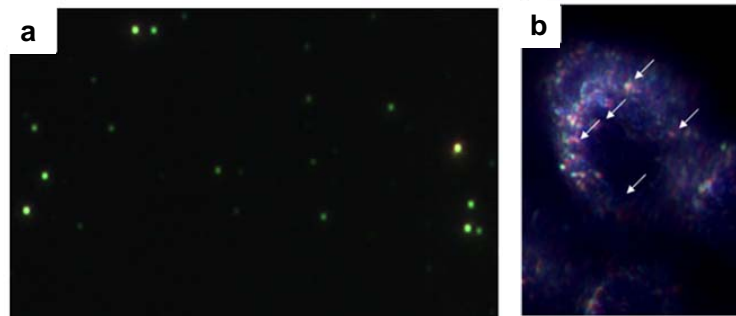


Figure 4. Scattering imaging of (a) 30-nm gold nanoparticles, (b) 15x 60 nm gold nanorods bound to HeLa cells.

- We tested their scattering imaging capabilities with 30-nm sized gold nanospheres and 15 x 60 nm nanorods. Figure 3b shows the scattering imaging of individual 30 nm gold nanospheres where each green spot represent plasmonic scattering of single gold nanosphere.

- We further performed feasibility test of their cellular imaging capabilities. Figure 4b shows gold nanorod labeled HeLa cells. Observation of intense red spots indicates successful scattering imaging of the nanorods attached on cells.

Conclusion

- We have successfully fabricated Mag-SPR probes (Mn-MEIO@SiO₂@Au).
- We have established successfully a high performance dark filed microscopic imaging system for the detection of single Mag-SPR nanoprobe.
- Feasibility test of single Mag-SPR probes imaging in cells was successfully performed.

The Final Report

Title: Electronic, Photonic and Magnetic Properties of Modified DNAs Complexed with Heavy Metal Ion

Principal Investigator:

DONG HOON CHOI (KPI, Korea University, Korea)

Telephone: +82-2-3290-3140

E-mail: dhchoi8803@korea.ac.kr

Contract Number: FA4869-07-1-4069

AOARD Reference Number: AOARD-074069

AOARD Program Manager: Sang-ho Byun

Period of Performance: 1 year

Submission Date: 8 Oct 2008

1st Year RESEARCH REPORT

◆ **Project Title:** Electronic, Photonic and Magnetic Properties of Modified DNAs Complexed with Heavy Metal Ion

◆ **Principal Researcher:** DONG HOON CHOI (KPI, Korea University, Korea)
A. J. Steckl (USPI, University of Cincinnati, USA)

Executive Summary

Program Goal: Understanding of mechanisms for charge transport, optical excitation/emission, magnetism of modified DNA.

Applications: Use modified DNA for electronic, photonic, and magnetic devices: BioLED, BioFET, BioSpinFET

Uniqueness: Aim to use unique structure of DNA double helix to develop devices with unique and superior characteristics.

Approaches: Collaboration between basic chemistry (KU) and device engineering (UC). KU is introducing intelligent functionality in DNA materials via synthetic approaches and UC is developing DNA thin films and novel device architectures based on the DNA materials.

Status and progress: at Korea Univ., new organic soluble DNAs were synthesized using various lipid unit. CTMA-DNA, Cz-DNA, and Chalcone DNA were employed to study their photophysical and photochemical properties. Mn-doped DNA was also used for studying the magnetism. At UC - Study of DNA thin films complexed with luminescent metalorganic compound (SRh) has yielded evidence of intercalation. UC collaboration also with AFRL-Materials Directorate (J. Grote, R. Naik) on materials properties.

Research during next period: At Korea University, phosphorescence and electrophosphorescence were studied using the Cz-DMA host after doping a soluble iridium complex we developed. Chalcone-DNA will be utilized as a dielectric layer for organic thin film transistor. In the field of magnetism, we will dope iridium complex or stable radicals to prepare the samples. At UC, Bio light emitting diodes (BioLEDs) incorporating DNA doped with SRh will be fabricated and characterized. Under our collaboration, the first co-work will be presented about photophysical properties of guest-host system or covalently bonded system.

1. INTRODUCTION

Among the rich world of naturally occurring biomaterials probably none is more important and more fundamental than **DNA** (deoxyribonucleic acid), the polymeric molecule that carries the genetic code in each living organism. It is not, therefore, not surprising that the nascent field of DNA photonics which combines *light* with the molecule of *life* excites the interest of the wider scientific community. Based on interaction of DNA with light, and with other segments of the electromagnetic spectrum, we can deduce the influence of electric and magnetic fields on the molecular unit in the DNA structure. Therefore, DNA is an ideal candidate for us to study electronic, photonic, and magnetic effects on biopolymers and to investigate related devices.

Organic and polymer chemists are able to introduce many intelligent functions in a material *via* various synthetic approaches. Electrical engineers are eager to exploit unusual material properties in designing novel or improved devices. However, an

optimum strategy is to combine the skills and interests of chemists and electrical engineers in order to take full advantage of the many hidden “talents” of DNA. By working together, the KU-UC team aims to reach the point where one can “tune” DNA such that it can display the desired specific properties for application to electronics, photonics, magnetism, biotechnology or other fields that have not been envisioned yet. That will indeed be a great accomplishment both in science and in technology.

2. VISION

This proposal aims to build an international collaboration between groups at Korea University (KU) and at the University of Cincinnati (UC) that are at the forefront of research on the properties of solid state DNA and application of these unique properties to novel devices.

3. GOALS/OBJECTIVES

- In-depth examination of the properties of solid state and modified DNAs.
- Application of modified DNA to electronic, photonic, and magnetic applications.
- Understanding of mechanisms for charge transport, optical excitation/emission and magnetism of modified DNA.

4. Researchers

◆ Principal Investigator(Korea): Dong Hoon Choi, Associate Professor

Department of Chemistry, KOREA UNIVERSITY, 5-1 Anam-dong, Sungbuk-gu, Seoul 136-701 KOREA

Professor: 2, Post Dr.: 1, Master Course Student: 1

◆ Principal Investigator(US): Andrew Steckl, Gieringer Professor, Ohio Eminent Scholar

Department of Electrical Engineering, UNIVERSITY OF CINCINNATI, 899 Rhodes Hall, Cincinnati Ohio 45221-0030 USA

Professor: 2, Post Dr.: 1, PhD student: 2

1.5 RESEARCH PROGRESS

A. Korea University

1.5.1. Organic Soluble DNA and its Analogues; Synthesis and Characterization of Chemical and Physical Properties.

The natural DNA can be dissolved in water and buffer, but not in the other organic solvents. For the thin film processing, the natural DNA must be modified to the soluble type. We synthesized CTMA-DNA, by reacting DNA with a cationic surfactant such as hexadecyltrimethyl ammonium bromide (CTMA). And also CTMA-polymethacrylic acid(PMA), CTMA-Polyglutamic acid were synthesized as reference materials.

The CTMA-DNA complex is used for the fabrication of thin film devices because they have a good solubility in alcohol. In addition, we also prepared functional lipids such as carbazolyl ammonium and chalcone-based ammonium etc..

(A) CTMA-DNA

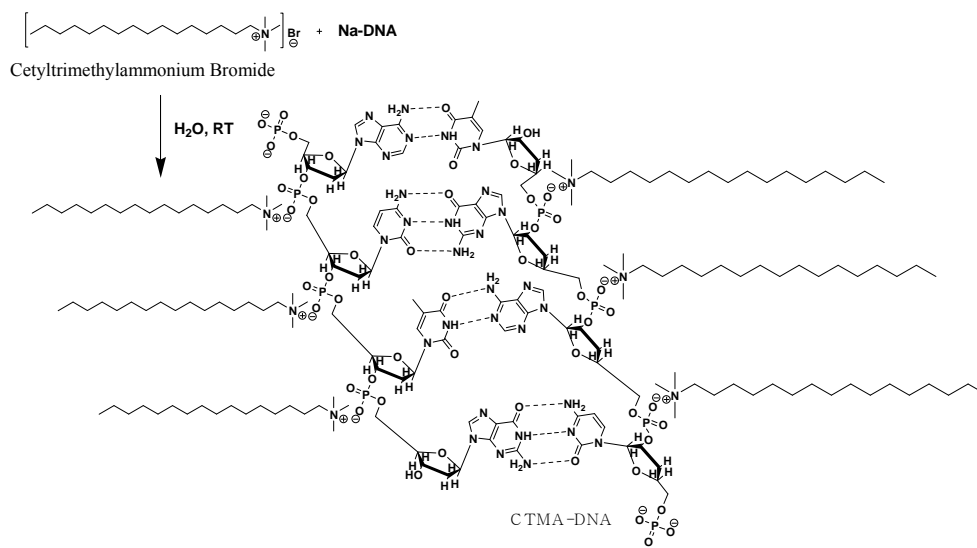


Figure 1. Synthetic procedure for CTMA-DNA

◆ To change the solubility, a cationic surfactant reaction was used to convert DNA to a DNA-lipid complex. Cetyltrimethylammonium bromide was used to form a DNA-CTMA complex as shown in Figure 1, which is not soluble in water but can be dissolved in alcohols and chloroform/EtOH mixtures.

Table 1. Transition metal ions and Metal impurities of CTMA-DNA

	Mn	Co	Ni	Cu	Fe	Na	Zn
Concentration (ppm)	<40.0	<40.0	<40.0	2334.6	<5ppm	<10ppm	<5ppm

◆ Transition metal ions and impurities were determined by the Korea Basic Science Institute (Seoul, Korea) using inductively coupled plasma-mass spectrometry (ICP-MS; ELAN 6000, Perkin-Elmer) and inductively coupled plasma Atomic Emission spectrometry (ICP-AES; Ultima 2C, Jobin Yvon Horiba). Resulting from this analysis, prior to the reaction, the concentration of sodium was 56770 ppm; after the reaction with CTMA, the concentration of sodium dropped to less than 10 ppm. Therefore, CTMA was substituted into the phosphate anion up to 99.5% or higher.

(B) Carbazole-DNA (Cz-DNA)

◆ Polyvinylcarbazole (PVK) is well known robust polymer that exhibits the high hole transporting mobility, high glass transition temperature, and good film forming property. It is quite effective since its highest occupied molecular orbital (HOMO) and triplet state energy levels almost coincide with those of conventional phosphorescence Ir(III) complex. Thus, Cz-DNA will be used for phosphorescence devices after doping new organic soluble Iridium complex. In this study, we also mimic the side chain of PVK and prepared carbazolyl ammonium salt for tethering it to phosphate anion. (See Figure 2 and 3)

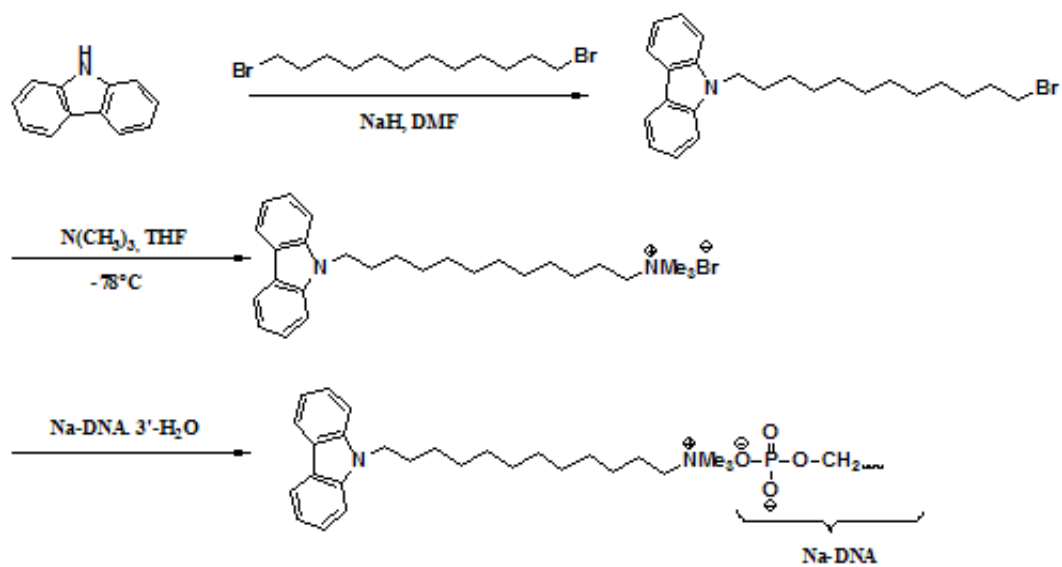


Figure 2. Synthetic procedure for Carbazole-lipid

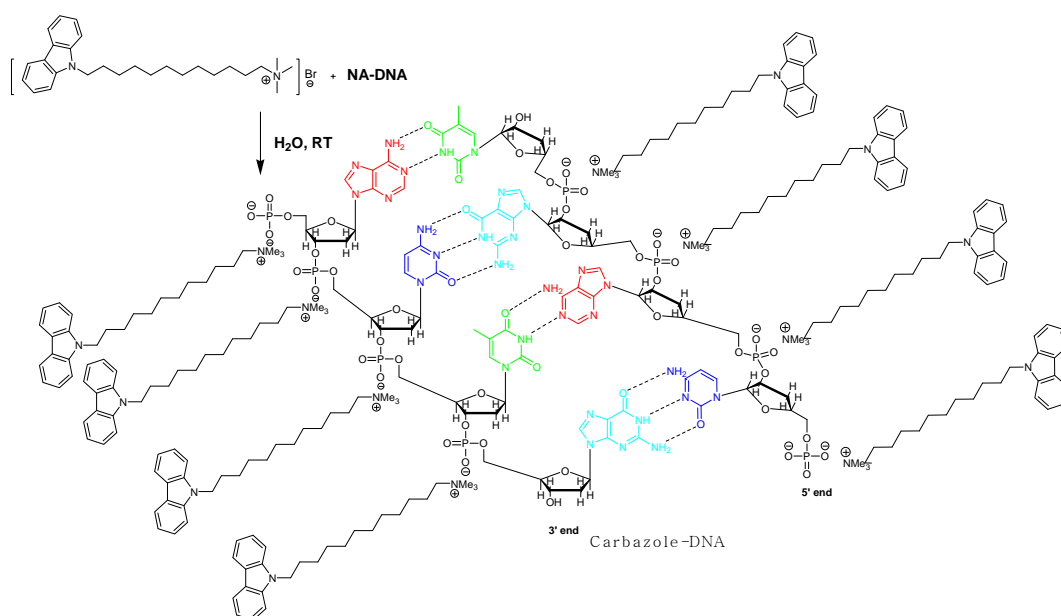


Figure 3. Synthetic procedure for Carbazole-DNA

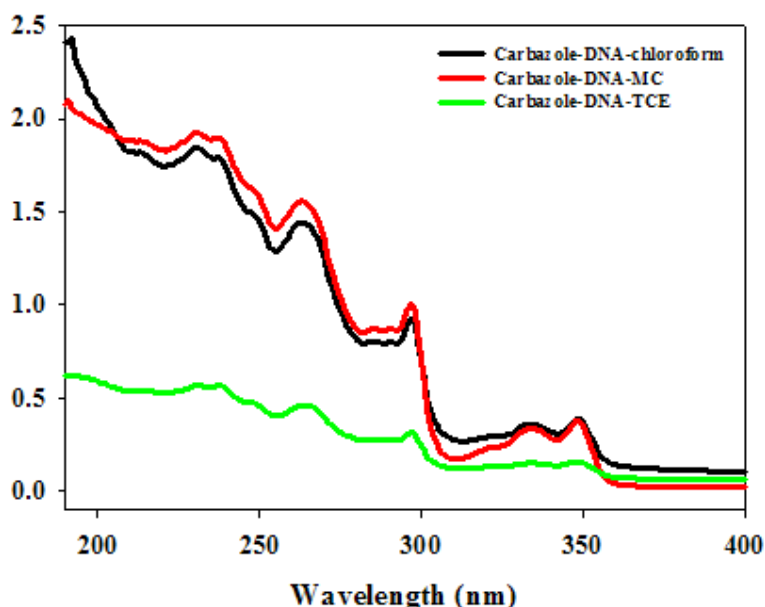


Figure 4. Absorption spectral analysis of Cz-DNA in different solvents.
 *Solvent: chloroform/EtOH mixture, MC(Methylene chloride), TCE(tetrachloroethane)

◆ A cationic surfactant reaction was used to convert DNA to a DNA-Carbazole-lipid complex. Carbazolyl ammonium bromide was used to form a carbazole-DNA complex as shown Figure 3, which is not soluble in water but can be dissolved in alcohols and chloroform/EtOH mixtures and many different solvents. In particular, the absorption spectrum of Cz-DNA is almost similar to that of PVK. The absorption band appeared at 340~350nm.

Table 2. Transition metal ions and impurities of Carbazole-DNA

	Mn	Co	Ni	Cu	Fe	Na	Zn
Concentration (ppm)	1885.5	147.7	7013.1	8585.9	133.7	423.8	76.00

◆ Transition metal ions and impurities were determined by the Korea Basic Science Institute (Seoul, Korea) using inductively coupled plasma-mass spectrometry (ICP-MS; ELAN 6000, Perkin-Elmer) and inductively coupled plasma Atomic Emission spectrometry(ICP-AES; Ultima 2C, Jobin Yvon Horiba). Resulting from this analysis, prior to the reaction, the concentration of sodium was 56770 ppm ; after the reaction with CTMA, the concentration of sodium dropped to less than 430 ppm. Therefore, Carbazolyl group was substituted into the phosphate anion up to 99% or higher.

(C) Chalcone-DNA: “Photoreactive DNA(negative resist)”

◆ Chalcone based polymer was a well-known photoresist since the chalcone group

easily undergoes 2+2 cycloaddition reaction. Photoproduct become insoluble in any organic solvent and patternability of this DNA is quite unique among many modified DNAs.

When we illuminate 360 nm of UV light, the crosslinking reaction is conducted. The synthesis is almost similar to the others. (See Figure 5)

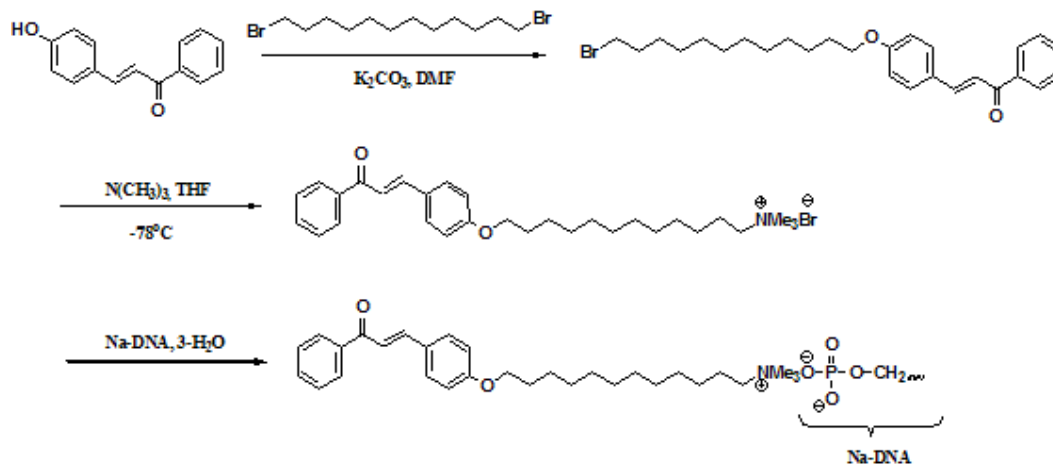


Figure 5. Synthetic procedure for chalcone-lipid.

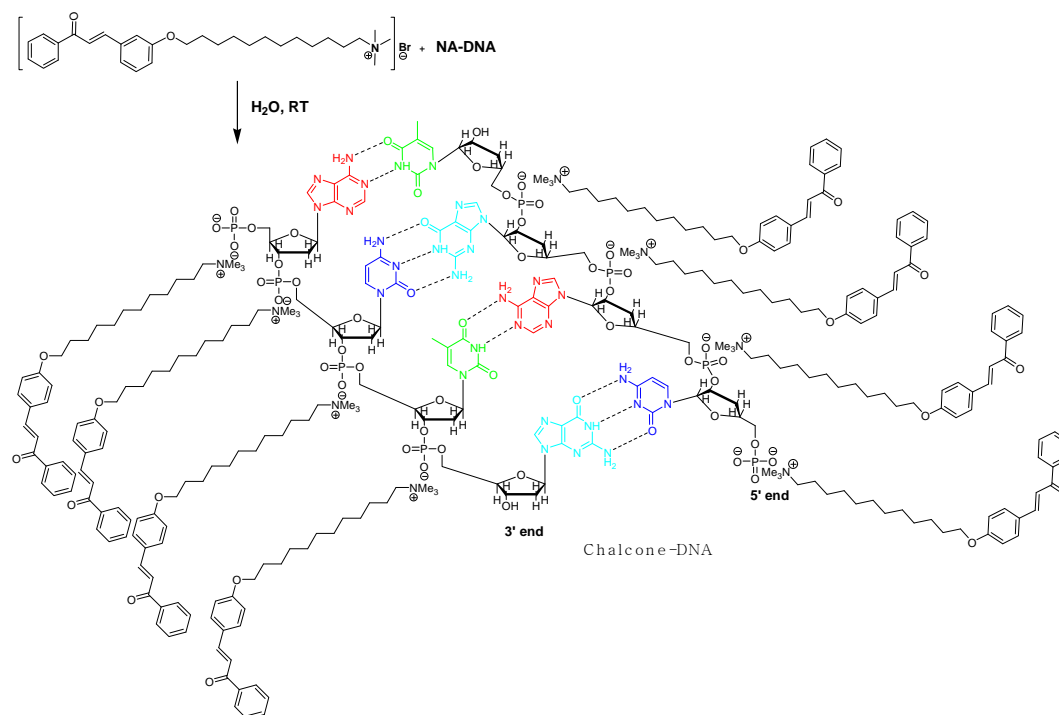


Figure 6. Synthetic procedure for DNA containing chalcone moiety in the side chain.

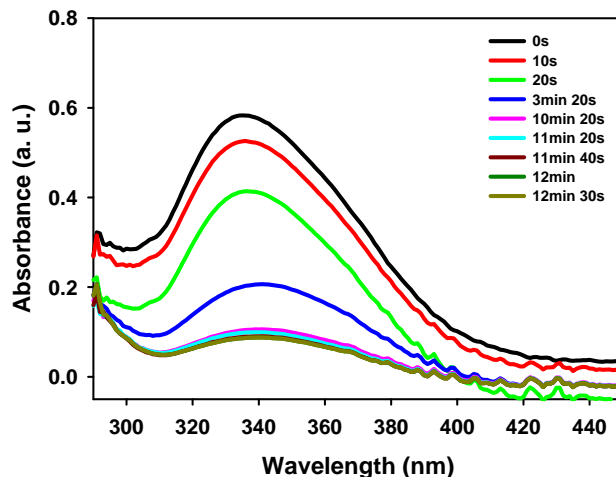


Figure 7. UV-Vis absorption spectral analysis of Chalcone-DNA with the irradiation time of UV light ($\lambda=365$ nm)

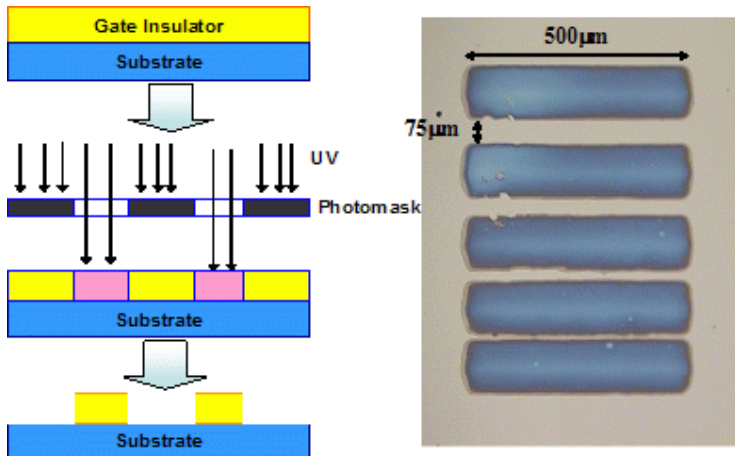


Figure 8. Photopatternability of Chalcone-DNA with the UV irradiation (Irradiation time: 100 sec at room temperature) ($\lambda=365$ nm)

◆ A functional cationic surfactant reaction was used to convert DNA to a DNA-Chalcone-lipid complex. Chalcone-based ammonium bromide was used to form a chalcone-DNA complex as shown Figure 5 and 6, which is not soluble in water but can be dissolved in alcohols and chloroform/EtOH mixtures and many different solvents. In Figure 7, the absorption spectral analysis displays the transition band at 365 nm. In Figure 7, we can observe the decrease of absorption at 360 nm with the irradiation time.

($\lambda=365\text{nm}$, Hg medium pressure lamp) We fabricate the pattern on the film of chalcone-DNA under a proper UV light dose. (see Figure 8)

► **Photoluminescence Study of CTMA-DNA doped with the DCM-based Fluorescent Molecules.**

We prepared the CTMA-DNA doped with DCM-based fluorescent dyes with a various concentrations and measured photoluminescence behaviors in solutions and dry film state. Enhancement of PL intensity was clearly observed.

◆ Purified natural DNA extracted from salmon sperm can only be dissolved in water; it is not soluble in any other organic solvent. Therefore, in this study, the structure of DNA was modified, and its solubility was changed. The preparation of organic-soluble DNA was carried out by precipitating the purified DNA in water with the cationic surfactant cetyltrimethylammonium chloride (CTMA). The resulting DNA-lipid complex shows good solubility in alcohol, which allows the fabrication of thin films for studying the photophysical properties of DNA in a solid state. The absorption and photoluminescence (PL) behaviors of CTMA-DNA and polymethylmethacrylate (PMMA) doped with (E)-2-(2-(4-(diethylamino)styryl)-4*H*-pyran-4-ylidene) malononitrile (DCM) were investigated. In addition, different PL spectral behaviors with differing concentrations of DCM in two different host materials were observed. These behaviors were explained by a mechanism based on intercalation or groove binding of fluorescent dye into the base pairs or aliphatic side-chain moieties of CTMA-DNA.

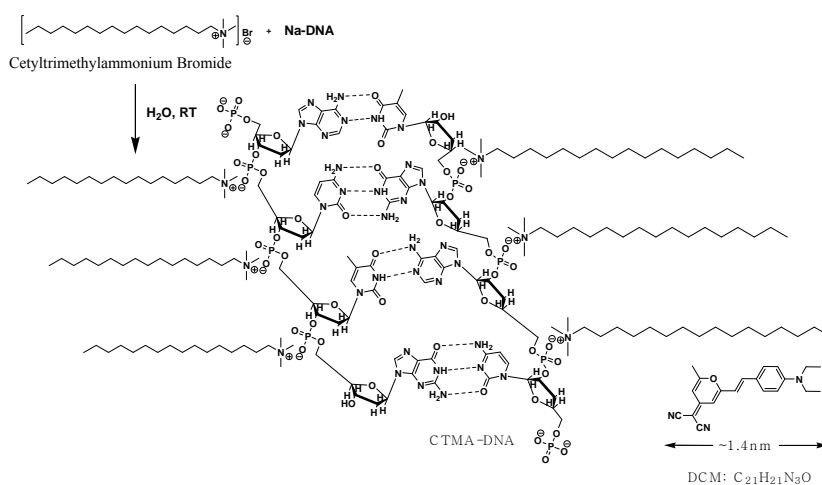


Figure 9. Synthetic procedure for CTMA-DNA and the structure of the DCM dye used in the present study

Absorption and Photoluminescence Behaviors

◆ The basic optical properties of the host-dye molecule thin films were characterized first, by determining the absorption and PL spectra for CTMA-DNA, DCM, and

CTMA-DNA doped with DCM (1 wt.%). (see **Figure 10**) CTMA-DNA exhibited the maximum absorption at approximately 260 nm, which is identical to that of water-soluble natural DNA. DCM dye itself exhibits a longer wavelength absorption in the range of 479 nm, which originates from the $\pi-\pi^*$ transition in the dye structure. After doping DCM dye (1 wt.%) into CTMA-DNA, the PL emission was observed at 567 nm, which is identical with that of DCM dye.

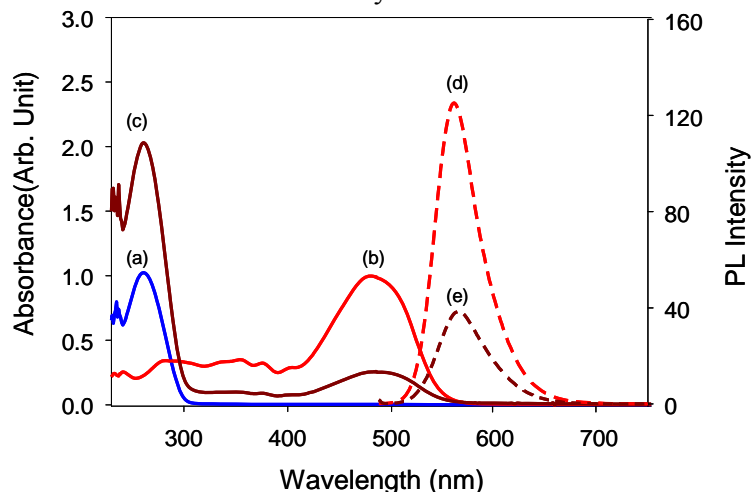


Figure 10. Absorption (solid lines) and PL spectra (dotted lines) of CTMA-DNA, DCM, and CTMA-DNA:DCM in solution states (chloroform, conc. 1×10^{-5} mole/L). (a) Absorption spectrum of CTMA-DNA, (b) Absorption spectrum of DCM, (c) Absorption spectrum of CTMA-DNA:DCM, (d) PL spectrum of DCM, and (e) PL spectrum of CTMA-DNA:DCM (1 wt.%).

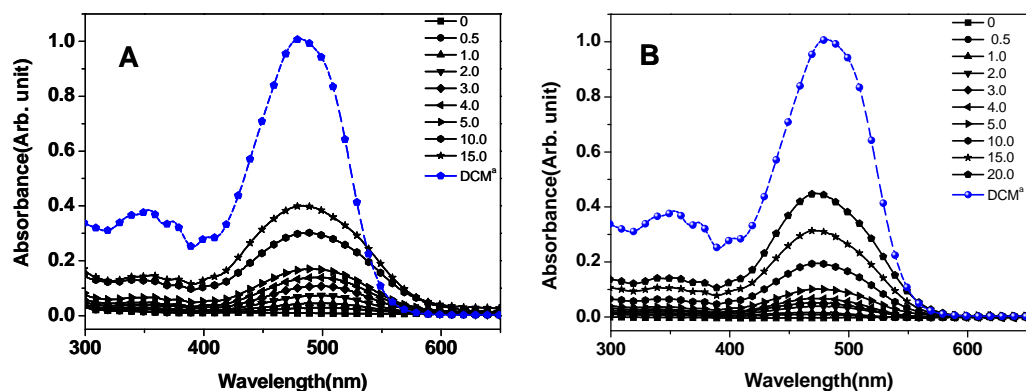


Figure 11. Absorption spectral behaviors of CTMA-DNA and PMMA doped with DCM dye; Effect of dye concentration (wt.-%) on the absorption spectral behaviors. *sample: thin film with an identical thickness. ($t \sim 100$ nm) A: CTMA-DNA $\lambda = 504-484$ nm. B: PMMA $\lambda = 465-472$ nm. ^a solution in chloroform

◆ The absorption spectrum of the DCM dye in chloroform was measured to show that the maximum absorption is at approximately 479 nm. A representative absorption set is shown in Figure 11. The CTMA-DNA film exhibits its well-known UV absorption peak

at 260 nm, owing to the presence of aromatic nitrogenous bases.

However, the film sample of CTMA-DNA with a low concentration of DCM dye exhibited a slight blue-shift from 504 nm to 484 nm ($\Delta\lambda=20$ nm), and the intensity increased monotonically with the concentration. The case of PMMA doped with DCM dye showed a slight red-shift, which is the opposite of the phenomenon in the CTMA-DNA sample. (465 nm \rightarrow 472 nm; $\Delta\lambda=7$ nm) When comparing the absorption maxima, the sample comprised of CTMA-DNA and DCM has lower energy absorption than that of the PMMA-doped sample, which is attributed to the polar environment from the amide bonds in the base pairs. In two samples, no severe aggregation behavior can be found in the spectra, indicating that DCM dyes are mono-intercalated into the base pair, which is supported by the similar interaction of cyanine dyes in the literature.

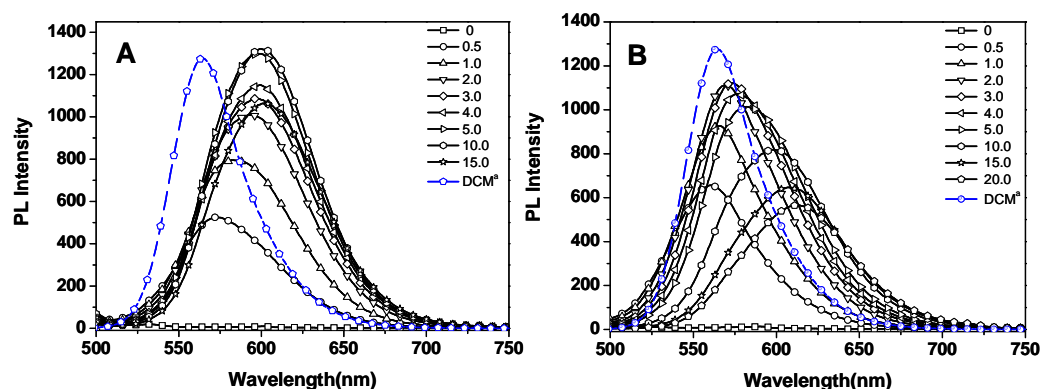


Figure 12. Photoluminescence spectral behaviors of CTMA-DNA and PMMA doped with DCM dye; Effect of dye concentration on the photoluminescence spectral behaviors. *sample: Thin film with an identical thickness. ($t\sim 100$ nm) A: CTMA-DNA $\lambda=504$ -484 nm. B: PMMA $\lambda=465$ -472 nm. ^a solution in chloroform

◆ To determine the optimal doping concentration for PL emission, CTMA-DNA and PMMA thin films containing a range of DCM concentrations were photoexcited at 488nm and 477nm, respectively. In Figure 12, the PL spectra of samples bearing different concentrations of DCM dye were compared. With a 0.5 wt.% concentration of DCM dye, the CTMA-DNA sample exhibited emission at 572 nm, which is shifted bathochromically. With increased concentration, the emission maximum shifted to 601 nm. Hence, the intensity of fluorescence was increased at a 10 wt.% concentration of DCM. The large shift of the emission center indicates that the polar character of the interior base pairs induced the effect, which is similar to solvatochromism in a solution state.

In the case of PMMA doped with DCM, the fluorescence begins to be quenched when the concentration is at 4 wt.%. The red-shift of the PL maximum of DCM-doped PMMA is observed with the increasing DCM concentrations, which can be attributed to the self-polarization of the red dopant. With an increasing dopant concentration, the distance between the DCM molecules decreases and the interaction is enhanced, which causes the red-shift in the PL spectra of the dopant. Under identical concentrations, the same shift behaviors were observed in DCM-doped polystyrene, which implies that the spectral shift is not affected by the polarity of the host matrix, rather by dye aggregation

or self-association. The fluorescence intensity of the CTMA-DNA:DCM sample increased continuously with the concentration of DCM dyes, due to chromophore isolation. Based on many studies, it can be conjectured that the isolation effect is attributed to groove binding or intercalation of dye through the base pairs. For instance, the intercalation of DCM dyes verifies the site isolation of the dyes when increasing the concentration to 10 wt.%. Almost no dye aggregation occurred at this high concentration, which is quite different from the guest-host system in common amorphous polymers such as PMMA and polystyrene. In addition, the fluorescent spectra show a significant red-shift in CTMA-DNA at a constant concentration (0.5 wt.%) ($\text{ca. } \Delta\lambda = 11 \text{ nm}$), which is attributed to the polarity of dsDNA. It is indicative of the charge transfer character of the fluorescent state.

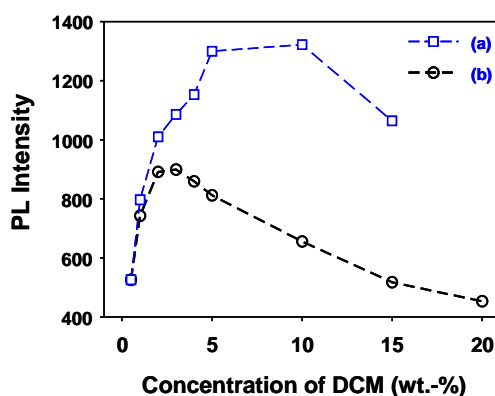


Figure 13. Integrated DCM photoluminescence vs. concentration in CTMA-DNA and PMMA. (a) CTMA-DNA-based films, (b) PMMA-based films.

◆ The thickness of the PMMA-doped film is slightly greater than those of the CTMA-DNA films ($t_{\text{CTMA-DNA}} = 0.86 t_{\text{PMMA}}$). At low concentrations ranging from 0.5 to 1.0 wt.%, two of the samples showed comparable PL intensity. The 3.0 wt.% DCM-doped PMMA showed the highest PL intensity, whereas continuous increments of the PL intensity of doped CTMA-DNA up to 10 wt.% were observed (see Figure 13). Generally, the PL intensities of the CTMA-DNA samples were higher than those of the PMMA-doped samples at high concentrations. It is consistent with the results reported in the literature, which describe intercalation-induced fluorescence enhancement [16].

It is interesting to consider the reasons behind the ability of the CTMA-DNA films to emit light more efficiently than other polymers. The intercalation or groove binding of certain fluorophores between the CTMA-DNA base pairs, which is frequently reported as a highly sensitive sign of the presence of CTMA-DNA molecules, could be the reason for the efficient luminescence. DCM may be more effectively prevented from intermolecular interaction when isolated by the base pairs in the CTMA-DNA structure. Furthermore, the tight spatial fit between DCM molecules and the base pair structure may retard the conformational relaxation of excited fluorophores and thereby enhance the process of radiative relaxation.

Temperature effect on Photoluminescence behavior of DCM-doped CTMA-DNA

◆ In order to investigate the origin of PL in DCM-doped CTMA-DNA, three samples

with different DCM concentrations were selected (ca. 1, 3, and 10 wt.%). In the PL spectra of DCM-doped CTMA-DNA taken at room temperature, the PL intensity have maximum value at the 10 wt.% DCM-doped film. When the PL spectra of DCM-doped CTMA-DNA (3wt.% or 10wt.%) were observed, three different binding modes of DCM dyes were expected: intercalation, groove binding, and external binding.

At the lowest temperature (18 K), clearer vibronic transitions were observed; emission peaks of DCM-doped CTMA-DNA (10wt.%) can be assigned to be 610, 667, and 715 nm. It should be noted that there is a significant difference in emission spectra between 300K and 18K. With an increase in the DCM dye concentration, the emission spectrum was transformed from the high energy to the low energy absorption region. Finally, at 10 wt.%, the doped DNA sample showed a clear shift of the maximum emission peak from 600 to 667 nm.

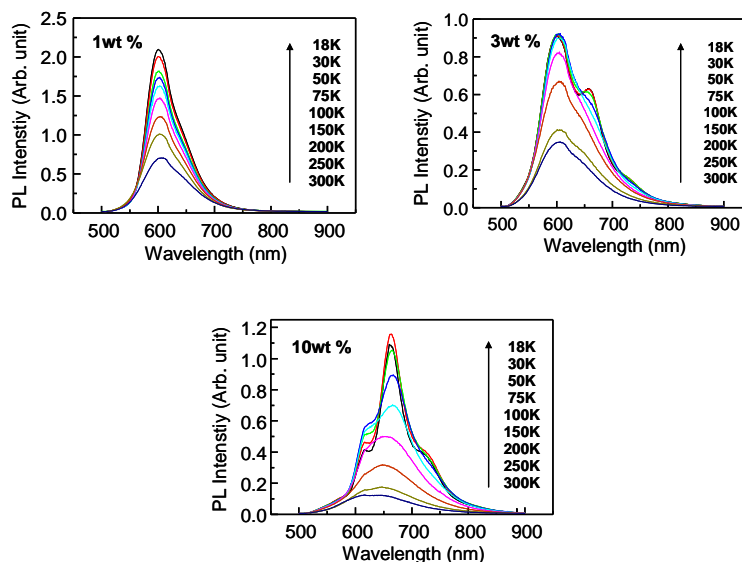


Figure 14. Temperature dependence of PL behaviors of CTMA-DNA in different concentration of DCM dye.

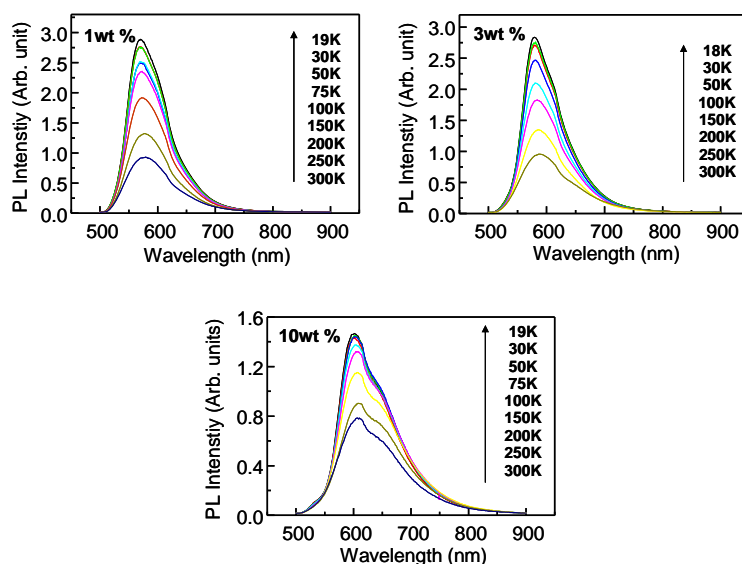
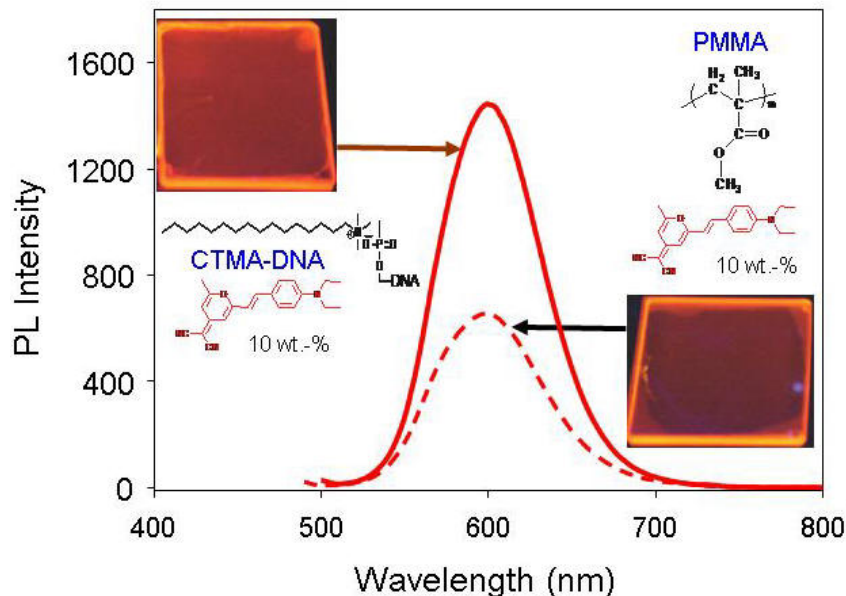


Figure 15. Temperature dependence of PL behaviors of PMMA in different concentration of DCM dye.

In contrast, when observing the same spectral behaviors of PMMA samples bearing DCM dye, the only difference in a heavily doped (10 wt.%) sample was the appearance of the PL emission at 640 nm as a shoulder; this is commonly understood to be due to the presence of intermolecular interactive species in the blend matrix.

◆ The peaks at around 600-610nm are commonly observed in the sample of DCM-doped CTMA-DNA and PMMA, which is attributed to the external binding of DCM dye around the polymer backbone. Below 100K of the CTMA-DNA sample, the gradual appearance of PL at 667 nm becomes evident as the PL emission at 610 nm gradually disappears. It was found that the DCM molecules in CTMA-DNA along with the base pairs undergo a different excited state under a polar environment. Such a large shift of the maximum emission wavelength can be attributed to the isolation effect of dyes in the CTMA-DNA matrix. The environment around the polar dye was significantly changed compared with that in the PMMA system, which implies that the DCM dyes were intercalated through the base pairs. The polar environment, which bears a high hydrogen-bond density, affects the transition dipole moment by changing the oscillating strength of the dye molecules. Then, the behavior is likely to mimic the solvatochromism in the solution state. At 18K, the dye molecules in CTMA-DNA become planar, which increases the conjugative effect. In the first-order excited state, the electrons are more highly delocalized, which induces the higher dipole moment than that of the ground state. Therefore, it facilitates the intercalation through the base pairs and shows a larger bathochromic shift of the spectrum.

Most DNA studies have been conducted using natural DNA in an aqueous-solution state; its unique properties have been intensely investigated for gene chemistry. CTMA-DNA is well-soluble in organic solvents such as alcohol and an alcohol/ halogenated solvents mixture. Organic-soluble non-ionic fluorescent dyes could easily be doped into CTMA-DNA without severe phase separation and crystallization. The photoluminescent behaviors of the two different dye-doped polymeric systems were investigated to understand the effect of dye concentration on the spectral shift behavior.



In particular, at a low concentration of DCM dye (~3 wt.%) embedded in PMMA, PL quenching behavior was observed to clarify the external binding effect or self-aggregation. However, DCM-doped CTMA-DNA samples do not show any PL quenching behaviors, even with a 10 wt.% concentration. No report has been made about the retardation of PL quenching at such a high concentration of polar fluorescent dye in the polymer matrix. Intercalation-induced PL enhancement and the isolation effect of dye molecules are quite unique in organic-soluble double-stranded DNA in a solid state. Although direct evidence resulting from general features of intercalation and the analytical evaluation of this binding mode are not present, a number of studies support the presented explanation.

► Magnetic Properties of Modified DNA with Heavy Metals

Earlier, we argued that only at low temperatures we could observe the appearance of the EMR peaks of Fe(III), whose content in the dry sample was about 30 ppm. One may ascribe the intrinsic magnetic properties of DNA to the presence of ferromagnetically interacting iron impurities. In this work we plan to study the magnetic properties of the modified DNA with iron ions (Fe^{3+}) to understand the intrinsic magnetic properties of natural DNA. This work is also expected to provide us with further insight on the magnetic properties of DNA-metal complexes.

SAMPLE PREPARATIONS

Salmon sperm ds-DNA sodium salts was purchased from Sigma-Aldrich Chemicals, Co., and used without further purification. Firstly, DNA was dissolved in the acetate buffer (pH 5.6) by stirring 24 hours and also the iron ion stock solution was prepared. And then 100 ppm and 500 ppm of iron (Fe^{3+}) chloride hexahydrate solution was pour into the DNA solution to obtain the DNA-iron complexes. DNA iron complexes were precipitated by the addition of the absolute ethanol into DNA solutions. Finally, each DNA-iron complexes was dried in the vacuum (1.0×10^{-2} torr) oven for 24 hours.

EXPERIMENTAL RESULTS

1. EPR measurement

EMR spectroscopy and SQUID magnetization measurements were employed to investigate the magnetic properties of the DNA samples because SQUID measures a bulk magnetization that is interpreted at the macroscopic level, whereas the EMR spectroscopic data can be analyzed in the molecular level. EMR spectroscopy was performed by using a Jeol JES-FA200 X-band spectrometer (9.1~9.5 GHz). The DC magnetic field was swept from 0 to 10000 G and the AC magnetic field modulation was applied at 5 G amplitude with 100 kHz. The receiver gain used was 5×10^2 .

Electron Paramagnetic Resonance spectra of DNA-Fe(III) complexes were shown in Figure 16 and we did not observe any significant change in the shape and intensities of EPR signals of the DNA-Fe(III) complexes having 100 ppm and 500 ppm iron ions. Therefore, we believe that the EPR signals of $g \sim 2.0$ are not originated from iron impurities and our future works are expected to clarify this point even further.

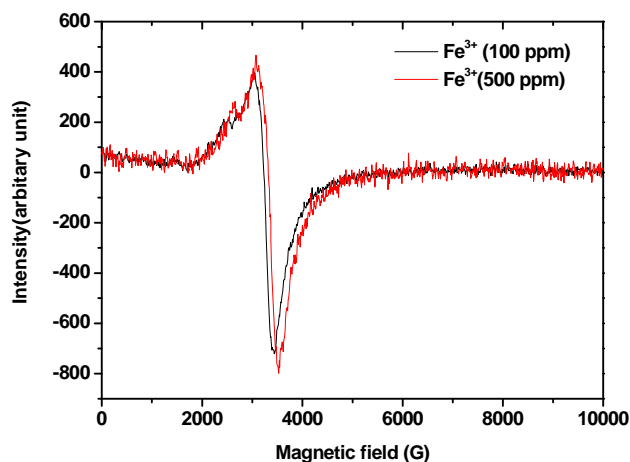
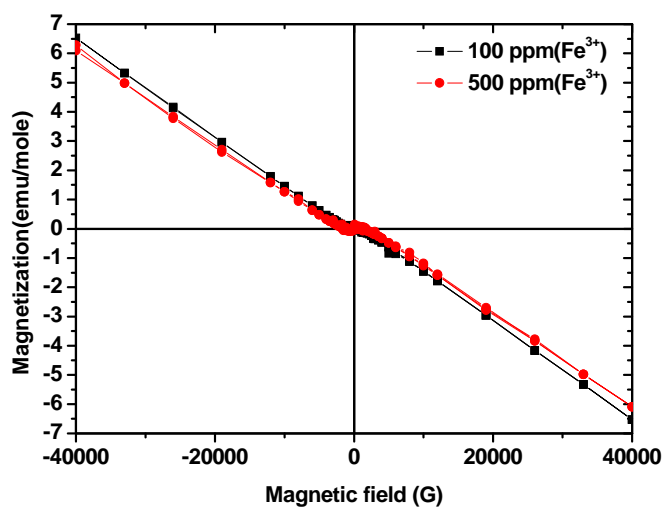
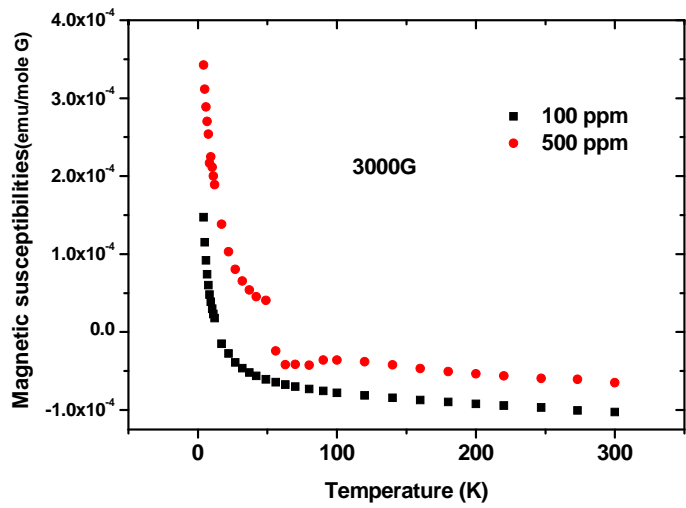


Figure 16. EPR spectra of DNA-Fe(III) complexes

2. SQUID measurement

SQUID (mpms 7, Quantum Design. Co., U. S. A.) magnetization data were collected with increasing temperature.



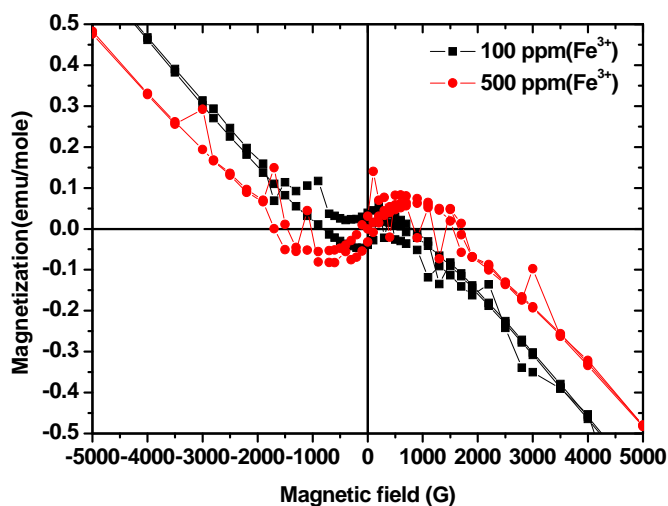


Figure 17. Temperature dependence and Magnetic field dependence of DNA-Fe(III) complexes.

Figure 17 shows SQUID results of the DNA-Fe(III) complexes. The M-H graph shows that DNA-Fe(III) complexes has very diamagnetic properties. However, there is a very small S-shaped signal from -3000 G to +3000 G and the maximum is around at 500~1000 G. Now, magnetic properties of DNA-Fe(III) complexes could not discuss in detail because experiments and analyses are not completed. However, we obtained the significant results from the EPR and SQUID; the EPR signals of DNA-Fe(III) complexes (100 ppm and 500 ppm) are same and the specific peaks were not observed. However, SQUID results show a small S-shaped signal. Therefore we need the further research to make a picture about the magnetic properties of DNA heavy metal complexes.

References

- [1] Watson JD, Crick FC. *Nature* 1953;171:737-8.
- [2] Steckl AJ. *Nat Photonics* 2007;1:3-5.
- [3] Stadler P, Oppelt K, Singh TB, Grote JG, Schwoediauer R, Bauer S, Piglmayer-Brezina S, Baeuerle H, Sariciftci D, Serdar N. *Org Electron* 2007;8:648-54.
- [4] Agen JA, Li W, Steckl AJ, Grote JG. *Appl Phys Lett* 2006;88:171109.
- [5] Condon A. *Nature reviews* 2006;7:565-75.
- [6] Erkkila KE, Odom DT, Barton JK. *Chem Rev* 1999;99:2777-95.
- [7] Armitage BA. *Top Curr Chem* 2005;253:55-76.
- [8] Lipscomb LA, Zhou FX, Presnell SR, Woo RJ, Peek ME, Plaskon RR, Williams LD. *Biochemistry* 1996;35:2818-23.
- [9] Ihmels H, Otto D. *Top Curr Chem* 2005;258:161-204.
- [10] Wood KC, Azarin SM, Arap W, Pasqualini R, Langer R, Hammond PT. *Bioconjugate Chem* 2008;19:403-5.
- [11] Patel S, Bui TT, Drake AF, Fraternali F, Nikolava PV. *Biochemistry* 2008;47:3235-44.
- [12] Grote JG, Diggs DE, Nelson RL, Zetts JS, Hopkins FK, Ogata N, Hagen JA, Heckman E, Yaney PP, Stone MO, Dalton LR. *Mol Cryst Liq Cryst* 2005;426:3-17.

- [13] Jun HS, Hong SY, Yoon SS, Kang CH, Suh MK. Chem Lett 2004;33:690-1.
 [14] Birch DS, Hungerford G, Imhof RE, Holmes AS. Chem Phys Lett 1991;178:177-84.
 [15] Tong Hui, Dong Y, Haußler M, Hong Y, Lam JY, Sung HH, Williams ID, Kwok HS, Tang BZ. Chem Phys Lett 2006;428:326-30.
 [16] Yu Z, Li W, Hagen JA, Zhou Y, Klotzkin D, Grote JG, Steckl AJ. Appl Optics 2007;46:1507-13.
 [17] Murphy CJ, Arkin MR, Ghatlia ND, Bossmann S, Turro NJ, Barton JK. Proc Natl Acad Sci USA 1994;1: 5315-9.
 [18] Holmlin RE, Tong RT, Barton JK. J Am Chem Soc 1998;120:9724-5.
 [19] Long EC, Barton JK. Accounts Chem Res 1990;23:271-3.

B. University of Cincinnati

Introduction

The unique structure of DNA has provided opportunities for novel and improved devices: photonics [1], electronics [2], spintronics [3], etc. We have previously reported [4, 5] the beneficial use of DNA nanometer thin films in OLEDs. Stimulated emission from lasing structures containing DNA gain medium doped with organometallic dye molecule sulphorhodamine (SRh) has shown quite a low threshold [6]. The SRh molecule is shown in Fig. 1. In the report period we have investigated the central issue of whether SRh is actually intercalated in the DNA structure and, conversely, whether the DNA structure, heavily loaded with SRh, preserves its chirality. Chirality of molecules is investigated by performing circular dichroism (CD) spectroscopy [7]. The sample to be considered is represented in the center of the CD spectrometer. Through this sample are passed beams of right and left circularly polarized light. In a sample that does not possess chirality (or handedness) there will be no difference in the intensity of the outgoing light. A sample with chirality will absorb, preferentially, either right or left polarized light. The difference observed between the intensity of the outgoing beams, is then correlated to the strength of the chirality of the sample and presented through a computer interface, as a CD spectrum. Since the DNA molecule exhibits chirality, it is clear that a CD spectrum will be present in the absorption region of DNA. Far less obvious is that a CD spectrum will be observed in the absorption region of the non-chiral SRh molecule, once combined with DNA.

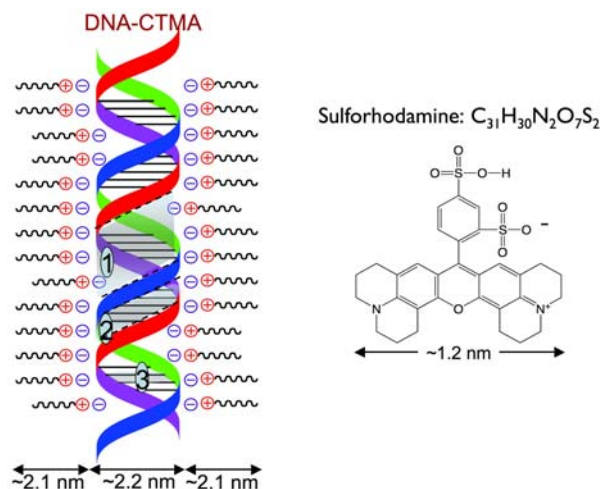


Fig. 1 The DNA-CTMA double helix polymer and the sulforhodamine molecule. The DNA double helix indicates possible locations for the binding of the SRh molecule: (1) major groove; (2) minor groove; (3) intercalation between base pairs.

Sample Preparation

CD spectroscopy experiments were performed both on liquid and thin film samples. The samples consisted of DNA:CTMA dissolved in butanol and combined with sulphorhodamine dye. The thin films were prepared from the same solutions used for the liquid samples in order to make comparisons between the two states more meaningful. Sample preparation is discussed for both, followed by an account of the CD experiments.

The liquid solutions were all 10% DNA:CTMA in butanol, by weight. This was dissolved on a rotary mixer, overnight, at room temperature. To each solution, sulphorhodamine was added in percentages of the weight of DNA:CTMA used. The solutions were each filtered through a 0.2 μm syringe-tip PTFE filter. Solutions of 0%, 2.5%, 5%, 10%, 15%, 20%, and 25% SRh to DNA:CTMA were prepared. Thin films produced via spin-coating were 1.5 μm in thickness.

CD experiments with solution samples were conducted by placing the liquid in a cylindrical cuvette with a liquid path length of 0.01mm. For DNA, the range 525-625 nm was scanned. For SRh, the range used was 220-340nm. The bandwidth was set to 15 nm and 5 nm for the DNA and SRh region, respectively. Background correction was performed, using a cuvette filled with butanol and noise was filtered from the results via the accompanying computer software.

For thin film scans, the samples used were spun on one half of the same type of cuvette as was used for the liquid samples. The CD signals observed for thin film samples were stronger than for the corresponding liquid samples in each case. This is because, despite the shorter path length of the thin films, those samples were more concentrated, due to the evaporation of the butanol.

Results and Discussion

CD signal is plotted against wavelength for four samples in Fig. 2. Considered here are samples containing DNA:CTMA only and those containing DNA:CTMA with 5 wt.% SRh. In this case, the CD signal is shown in the DNA absorption region. Results for both thin film and solution samples are included. Here, there is no obvious correlation between the presence of SRh and the strength of the DNA CD signal. The strength of the signals for the thin film samples are stronger than those of the solution samples. This is typical of our samples due to the concentrated nature of the thin films, putting more material in the path of the CD spectrometer.

In Fig. 3, a similar plot is provided, but for the SRh absorption wavelength region. Displayed here are spectra for samples containing 2.5% and 15% SRh to DNA:CTMA by weight. Both thin film and solution spectra are provided. It is, again, observed that the thin films result in a CD spectrum of greater intensity than the solution samples. Notable, is the increase in amplitude with an increase in SRh concentration, for both thin film and solution cases.

A summary of the peak-to-peak CD amplitude (in the DNA absorption region) of the samples investigated is shown in Fig. 4. There is no obvious correlation in solution samples, between SRh concentration and DNA CD intensity. For thin films, the CD

signal demonstrates a slight increase in intensity, in combination with SRh, with the exception of a decrease in signal at the highest concentration (25%) of SRh. It is possible that enough SRh molecules are finally attached to the DNA molecule, in the this case, to begin disturbing the chirality of the spiral.

Figure 3 also shows peak-to-peak CD amplitude in the SRh absorption region. Here, there is a clear increase in CD signal strength, with increasing SRh concentration. This observation demonstrates that SRh takes on the chiral nature of the DNA molecules with which it has been combined. The plot flattens at higher concentrations of SRh, indicating a saturation effect, wherein the sample contains more SRh than can readily bind to the DNA.

Summary of Current Results

We have considered the important question of the physical nature of the association between DNA and SRh.

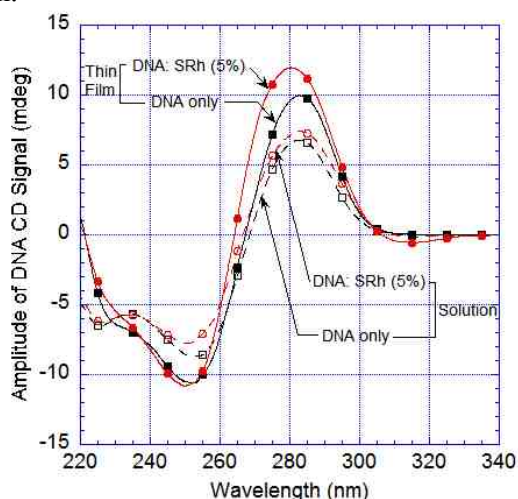


Fig. 2 CD signal (mdeg) for SRh absorption region vs wavelength (nm). DNA only and DNA:SRh 5% are included in both solution and thin film forms.

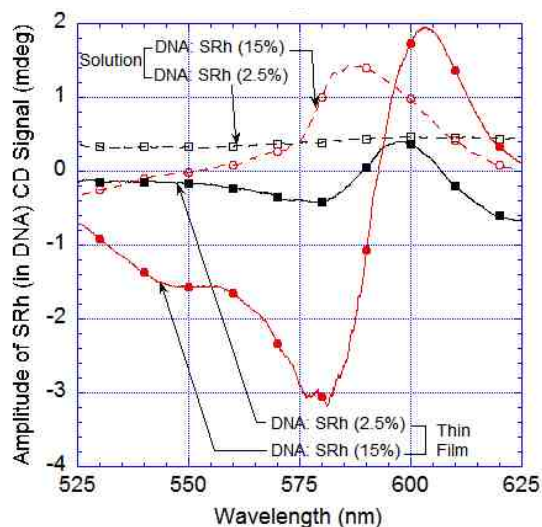


Fig. 3 CD signal (mdeg) for DNA absorption region vs wavelength (nm). DNA only and DNA:SRh 5% are included in both solution and thin film forms.

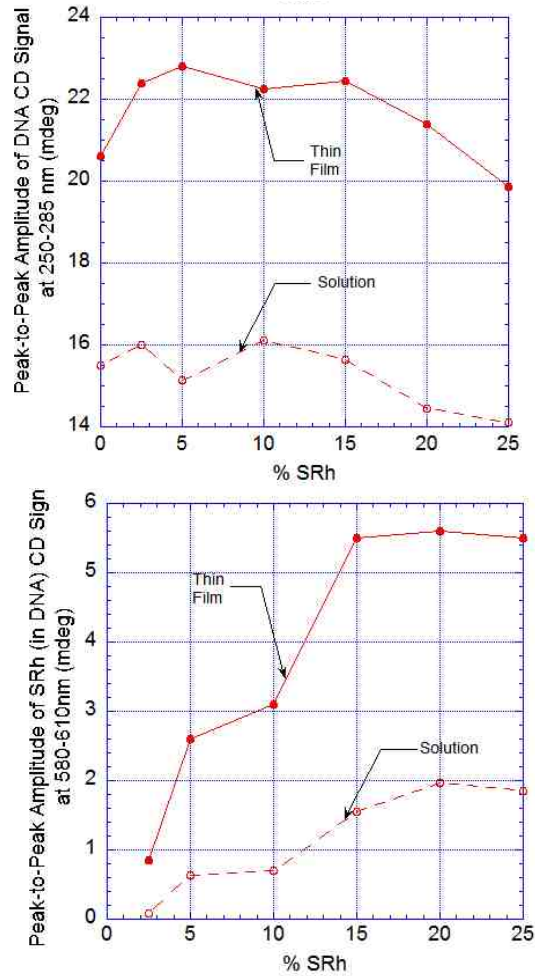


Fig. 4 Peak-to-peak CD Signal (mdeg) for SRh and DNA regions versus SRh concentration (%).

In doing so, we have used CD spectroscopy to demonstrate that SRh takes on the chiral nature of DNA in a mixture and, thus, is intercalated in the DNA. Also, it has been shown that this intercalation enhances the natural chirality of the DNA molecule, below a SRh concentration of 25% in thin films.

- [1] A. J. Steckl, "DNA - a new material for photonics?," *Nature Photonics*, vol. 1, p. 3, January 2007 2007.
- [2] B. Singh, N. S. Sariciftci, J. Grote, and F. K. Hopkins, "Bio-organic-semiconductor-field-effect-transistor based on deoxyribonucleic acid gate dielectric," *Journal of Applied Physics*, vol. 100, p. 024514, 2006.
- [3] C. H. Lee, E.-D. Do, Y.-W. Kwon, D.-H. Choi, J.-I. Jin, D.-K. Oh, H. Nishide, and T. Kurata, "Magnetic Properties of Natural and Modified DNAs," *Nonlinear Optics, Quantum Optics*, vol. 35, pp. 165-174, 2006.
- [4] J. A. Hagen, W. Li, A. J. Steckl, and J. G. Grote, "Enhanced emission efficiency in organic light-emitting diodes using deoxyribonucleic acid complex as an electron blocking layer," *Applied Physics Letters*, vol. 88, p. 171109, 2006.
- [5] J. A. Hagen, W. X. Li, H. Spaeth, J. G. Grote, and A. J. Steckl, "Molecular

- Beam Deposition of DNA Nanometer Films," *Nano Lett.*, vol. 7, pp. 133-137, 2007.
- [6] Z. Yu, W. Li, J. A. Hagen, Y. Zhou, D. Klotzkin, J. G. Grote, and A. J. Steckl, "Photoluminescence and lasing from DNA thin films doped with sulforhodamine," *Applied Optics*, vol. 46, p. 7, 20 March 2007 2007.
- [7] A. Rodger and B. Norden, *Circular Dichroism & Linear Dichroism*. Oxford: Oxford University Press, 1997.

1.6 Summary

This research is based on collaboration between Korea University (KU) and the University of Cincinnati (UC). The topic of the research is the investigation of the electronic, photonic and magnetic properties of DNA and the use of the unique properties of DNA in developing novel and improved devices. Researchers of Korea University are introducing many intelligent functions in a natural DNA *via* various synthetic approaches. UC are trying to exploit unusual material properties in designing novel or improved devices.

Now, DNA-surfactant complexes themselves and DNA-surfactant complexes doped with fluorescent or phosphorescent dyes were prepared by Korean Researchers, but characterization of chemical and physical properties are now under way. Fe-DNA, Mn-DNA and Mg-DNA were prepared and Electron Spin Resonance Spectroscopy (ESR) was performed to study on the magnetic properties. And also UC tried to make a various devices with MBD technique and are obtaining the current-voltage (I-V), current-light (I-L), and light-time (L-t) characteristics and so on.

The Final Report

Title: Hierarchical Carbon Fiber Composites

Principal Investigator:

Professor Kun-Hong Lee, Department of Chemical Engineering,

POSTECH

Telephone: +82-54-279-2271

E-mail: ce20047@postech.ac.kr

Contract Number: FA4869-07-1-4069

AOARD Reference Number: AOARD-074069

AOARD Program Manager: Sang-ho Byun

Period of Performance: 1 year

Submission Date: 8 Oct 2008

Hierarchical Carbon Fiber Composites

KPI : Kun-Hong Lee, Ph.D. (POSTECH)

Co-KPI : Sang-gi Lee, Ph.D. (Ehwa Women's University)

USPI : H. Thomas Hahn, Ph.D. (UCLA)

Final Report

Research Title: Hierarchical Carbon Fiber Composites Task I: Formation of nanostructures on the surfaces of carbon fibers

Research Institute: Department of Chemical Engineering, POSTECH

Principal Investigator: Professor Kun-Hong Lee

Co-Investigator: Dong-Myung Yoon and Eugene Oh

1.1. Objective

The first-year aim of Task I is to form carbon nanotubes (CNTs) on the surface of carbon fibers (CFs) to develop hierarchical carbon fiber composites.

1.2. Status of Effort

A thermal chemical vapor deposition(CVD) method has been established as a conventional approach to form a homogeneous structure of carbon nanotubes on carbon fiber fabric. The microwave irradiation method, a patented technique, has also been used successfully.

1.3. Accomplishments (Related data: Appendix A)

Figure 1 shows the formation of CNTs on the surface of carbon fiber fabric from three different types of carbon sources.

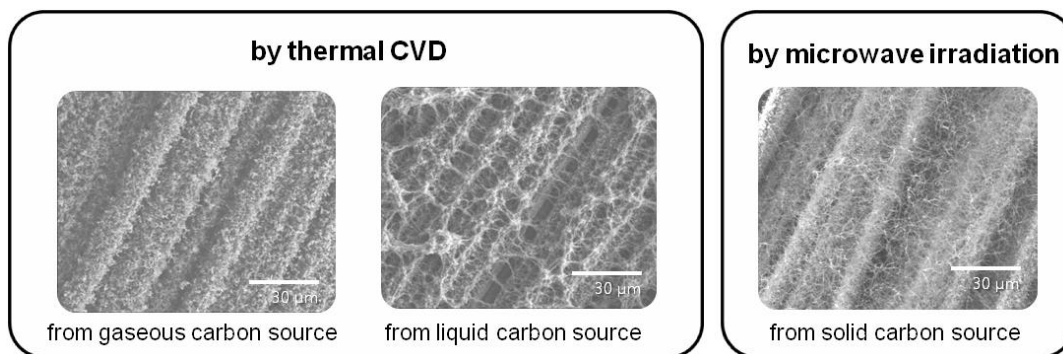


Fig. 1. Growth of carbon nanotubes(CNTs) on the surface of carbon fibers.

Growth of carbon nanotubes on the surface of carbon fibers was investigated by **thermal CVD method** which is amenable for large-scale synthesis. C_2H_2 , a **gaseous carbon source** was used as the reactant in Figs. 2(a), (b), (c), and (d), and they show homogeneous formation of fibrous nanostructures of 30~100 nm diameters on the surfaces of carbon fibers. Figure 2(d) proves that this fibrous nanostructure has a hollow core. Change of reactant to ferrocene and xylene, a **liquid carbon source**, results in longer nanostructures in larger amount as shown in Fig. 2(g). These samples were supplied to Prof. Sang-gi Lee (Ehwa Women's University) and Prof. Hahn (UCLA) for surface modification and composite fabrication, respectively.

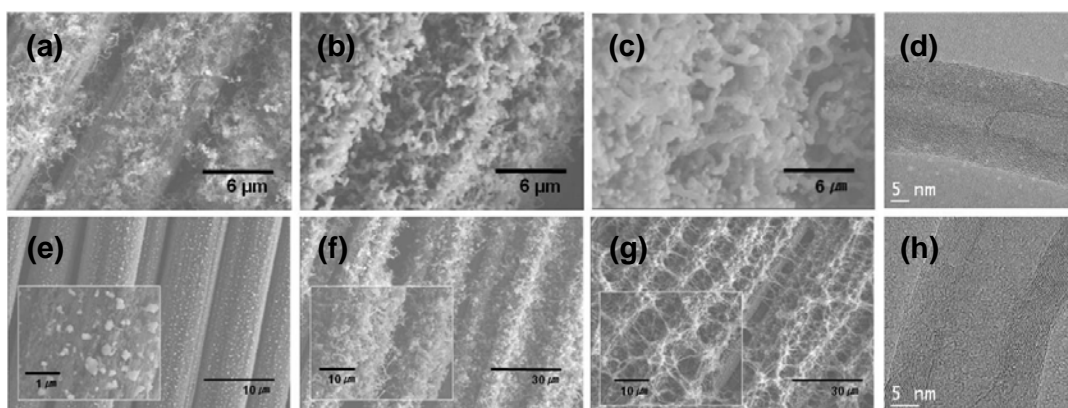


Fig. 2. Two types of CNT growth on carbon fibers using thermal CVD. (a), (b), and (c) at 800 °C for 10 min under 160 sccm Ar gas and 40 sccm C_2H_2 gas with 3 nm, 10 nm, and 50 nm Ni catalyst depositions, respectively. (e), (f), and (g) at 850 °C for 90 min under 185 sccm Ar gas and 15 sccm H_2 gas with 6.5 mol% ferrocene and 100 mol% xylene. The flow rate was (e) 0.195 ml/hr, (f) 0.98 ml/hr, and (g) 1.95 ml/hr. (d) and (h) are HR-TEM images of (a) and (g).

We also obtained in situ formation of CNTs on carbon fibers by using the carbon fibers as a **solid carbon source in the microwave synthesis**. The irradiation time was only one minute. Previous researchers have commonly made use of hydrocarbon vapors or liquid carbon sources, but our group investigated the feasibility of a direct transformation from a solid carbon source. Carbon fiber fabric was sputtered with nickel to form a thin nickel film, and the sample was irradiated with a microwave power of 2000 W. When 2.45 GHz microwave was directly irradiated on the nickel catalyst layer, the

layer was heated and was transformed into isolated islands. Carbon atoms could evaporate from carbon fibers, caused strong microarcs on the surface of the catalyst islands. We examined the changes on the surfaces of carbon fibers in the different conditions to find the optimum process window as Appendix A. Figure 3(a) shows CNTs grown in situ on a carbon fiber. These CNTs could be divided into Ni filled tubes, Fig. 3(b), and empty tubes with a graphitic shell, Fig. 3(c).

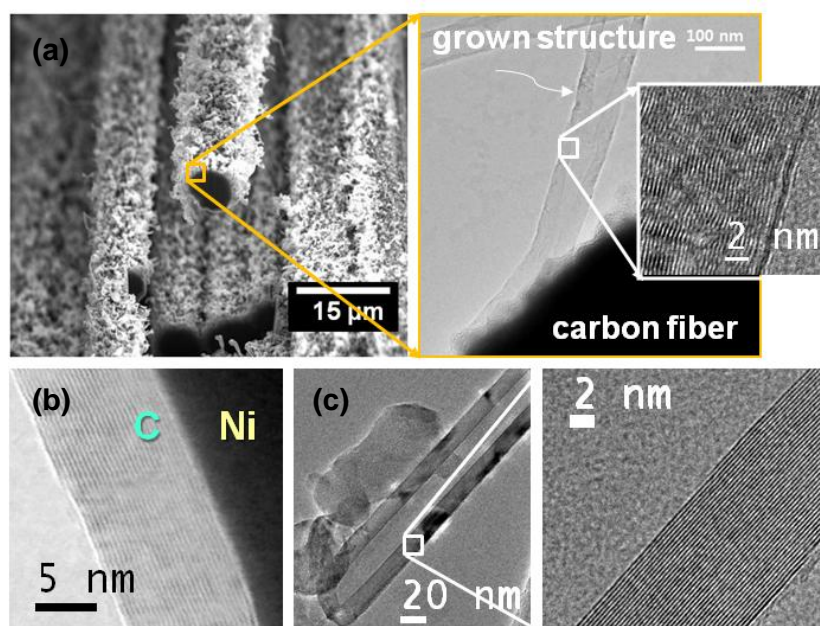


Fig. 3. CNT growth on carbon fibers using Microwave Irradiation System. (a) at 2000 W for 40 sec under 180 sccm Ar gas and 20 sccm H₂ gas with 50 nm Ni catalyst deposition. (b) Ni filling inside a CNT. (c) a CNT with well-aligned concentric layers.

Research Title: Hierarchical Carbon Fiber Composites Task II: Ionic liquid-carbon nanotube hybrid materials

Research Institute: Division of Nano Sciences/Department of Chemistry, Ewha Womans University

Principal Investigator: Professor Sang-gi Lee

Co-Investigator: Dr. Yu Sung Chun, Ju Yeon Shin and Cho-Long Park

2.1. Objective

The aim of the research project is the development of hierarchical carbon fiber composites through the covalent modification of carbon nanotubes with ionic liquid moiety having a polymerizable functional group.

2.2. Status of Effort

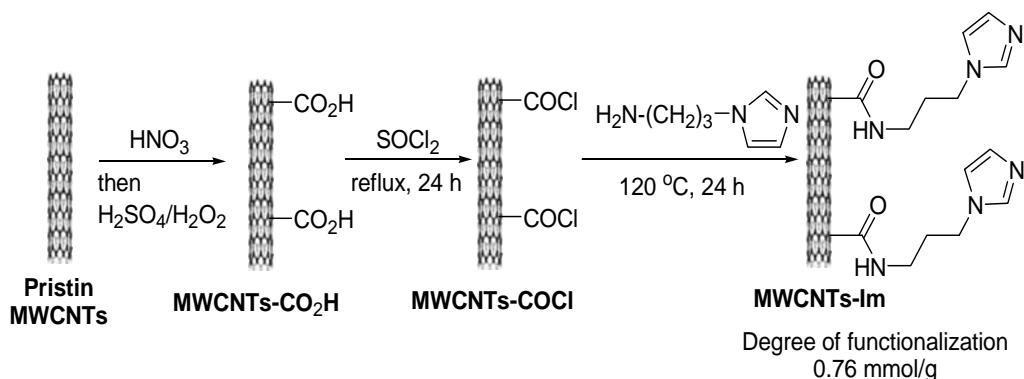
Functionalization methods for multi-walled carbon nanotubes with polymerizable ionic norbonene and ionic epoxide functional groups have been established.

2.3. Accomplishments

2.3.1. Preparation of imidazole-functionalized MWCNTs

We have developed functionalization methods for ionic liquid-carbon nanotubes having polymerizable norbonene and epoxy functional groups, Fig. 4. The pristine multi-walled carbon nanotubes (MWCNTs) were oxidized by HNO_3 followed by washing with Piranha solution to synthesize carboxylic acid-functionalized MWCNTs (MWCNTs-COOH). The carboxylic acid group was converted to acid chloride (MWCNTs-COCl) by treatment with excess amount of SOCl_2 after 24-h reflux. The resulting MWCNTs-COCl reacted with commercially available 3-aminopropyl imidazole at 120°C for 24 h under nitrogen atmosphere. The resulting black solid was filtered through a 0.2-micron poly(tetrafluorethylene) (PTFE) membrane, and successively washed with anhydrous tetrahydrofuran (THF) followed by 1-M aqueous HCl solution, saturated NaHCO_3 solution, and water until the pH of the filtrate was 7.0. Elemental analysis indicated 0.76 mmol/g of imidazole moiety was incorporated into the CNT surface. To introduce the epoxy group, the imidazole-

functionalized CNTs were reacted with an excess amount of epichlorohydrine at 90°C for 48 h. After filtration, the resulting ionic liquid-functionalized CNTs (MWCNTs-Im) with epoxy group were washed several times with acetonitrile, and dried under vacuum at 60°C for 24 h. These ionic-liquid

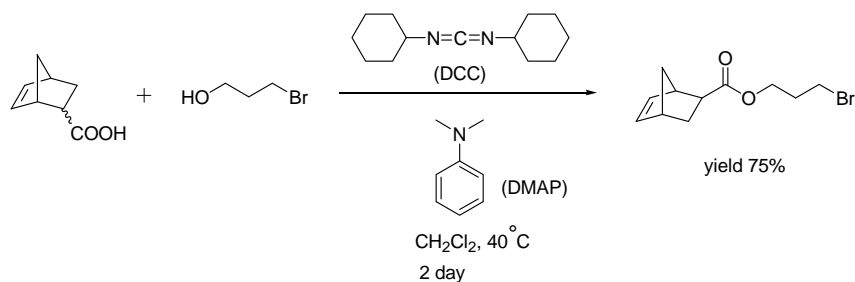


functionalized CNTs (CNT-ILs) were to be used to fabricate CNT-ILs/epoxy nanocomposites.

Fig. 4. Imidazole functionalization of MWCNTs.

2.3.2. Synthesis of Brominated norbornene

The brominated norbornene was synthesized by reacting 5-norbornene-2-carboxylic acid with bromopropanol using dicyclohexylcarbodiimide as a coupling agent with a 75% yield, Fig. 5.



$^1\text{H NMR}$ (250MHz, CDCl_3): δ 1.27-1.30 (m, 1H), 1.40-1.46 (m, 2H), 1.91-1.92 (m, 1H), 2.14-2.21 (m, 2H), 2.92-3.00 (m, 2H), 3.20 (s, 1H), 3.44-3.50 (t, 2H, $J=6.6$), 4.13-4.23 (m, 2H), 5.91-5.94 (q, 1H, $J=2.8$), 6.19-6.22 (q, 1H, $J=2.8$).

Fig. 5. Synthesis of brominated norbornene.

3.3 Preparation of polymerizable ionic MWCNTs having norbornene and epoxy functional groups

The imidazole-functionalized MWCNTs-Im were reacted with excess amounts of commercially available epichlorohydrin and brominated norbornene in CH_3CN for 36 h and 48 h, respectively. The chloride and bromide anions were exchanged to PF_6^- anion, Fig. 6. Figure 7 shows TEM micrographs of functionalized MWCNT-IL(PF_6^-)-epoxy and MWCNT-IL(PF_6^-)-norbonene.

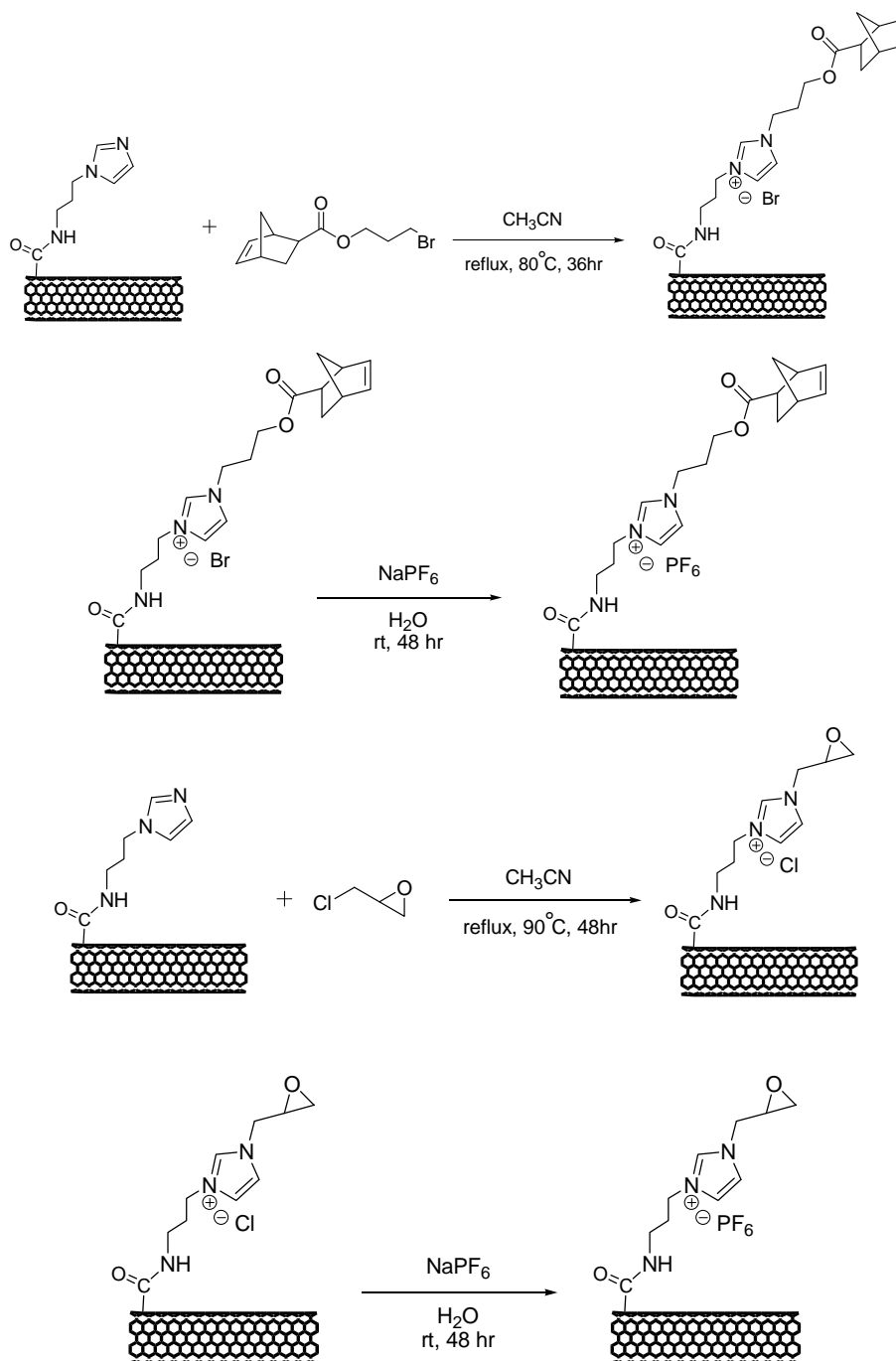
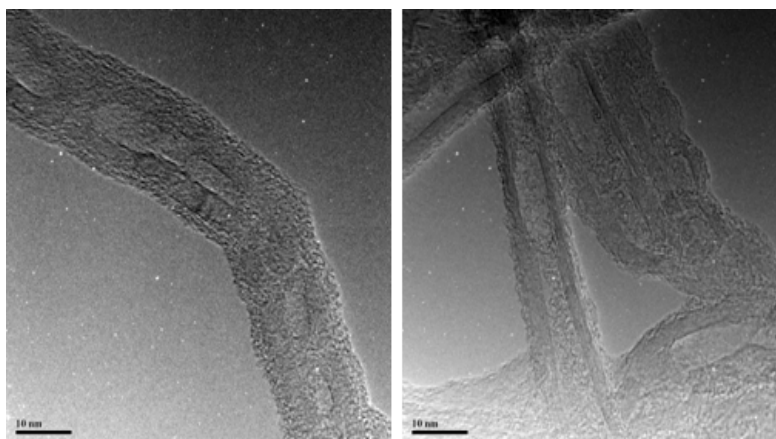


Fig. 6. Synthesis of MWCNTs with norbonene and epoxy groups.



(a)

(b)

Fig. 7. TEM images of functionalized MWNT-IL(PF₆): (a) epoxy and (b) norbonene.

Research Title: Hierarchical Carbon Fiber Composites Task III: Composite processing and characterization

Research Institute: Mechanical & Aerospace Engineering Department, UCLA

Principal Investigator: Professor H. Thomas Hahn

Co-Investigator: Dr. Zhe Wang

3.1. Objective

The aim of Task III is to develop processing methods for hierarchical carbon fiber composites and characterize their mechanical and electrical properties.

3.2. Status of Effort

Preliminary processing methods have been established to fabricate epoxy resin composites using CNTs functionalized in Task II. The effects of processing on mechanical and electrical properties were studied. The conductivity data shows a large improvement resulting from both ionic liquid functionalizations. An optimization process has been established to fabricate one layer CNT-carbon fiber/epoxy composite. CNTs grown on carbon fibers have been found to increase the hierarchical composite conductivity.

3.3. Accomplishments

3.3.1. Preparation of MWCNT-IL/epoxy composites

We have fabricated nanocomposites using PF₆-ionic liquid-functionalized MWCNTs, MWCNTs-IL(PF₆)-epoxy, obtained from Task II. The functionalized MWCNTs were first added to DETDA curing agent (Epicure W), sonicated and then mixed with the base DGEBF epoxy resin (Shell Epon 262). The expected cure mechanisms are shown in Fig. 8.

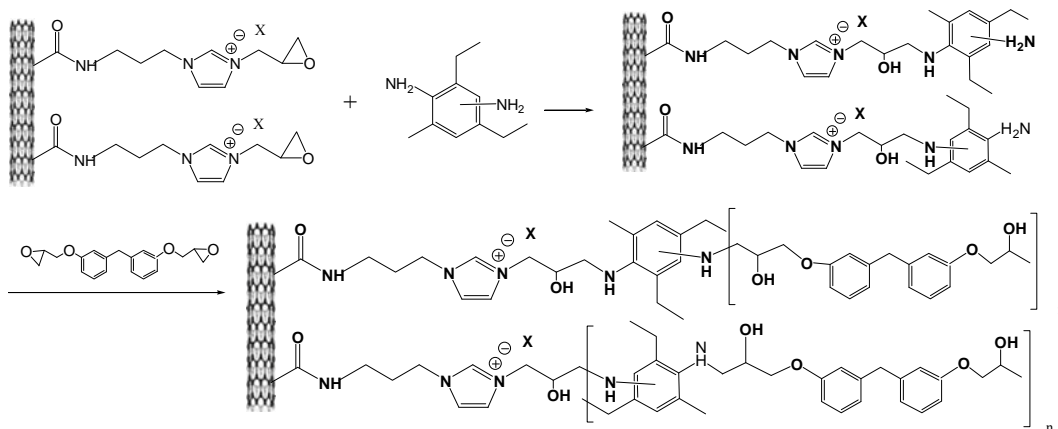


Fig. 8. Synthesis route MWCNT-IL(X)-epoxy/epoxycomposite (X: Cl and PF6).

3.3.2. PF₆-CNT/Epoxy composite

Processing has been varied to find an optimum process to yield best properties. In total six different processes have been tried and Table 1 shows the results. The best process requires the use of a mixed solvent and involves the following steps:

- (1) Add MWCNTs into a mixed solvent (dichloromethane+acetone+THF) and sonicate for 6 h.
- (2) Add curing agent and sonicate for 3 h at 60°C
- (3) Add a small amount of epoxy (1/4 curing agent) and sonicate for 2 h at 60°C.
- (4) Evaporate solvent in vacuum for 1 h at 80°C and then for 1 h at 100°C.
- (5) Add remaining epoxy, stir for 0.5 h and sonicate for 1 h.
- (6) Degas in vacuum for 0.5 h at 60°C and then for 0.5 h at 80°C.
- (7) Pour into mold and cure for 4 h at 120°C.

This process is designated as Process VI in Table 1.

Table 1. Processing effect on MWCNT-IL(PF₆)/epoxy composite properties

Content, wt%	0		0.1		0.5		1.0	
Process	Strength MPa	Conduct. S/cm						

I	78.9	$<10^{-12}$	86.0	N/A	94.8	N/A	96.7	N/A
II	85.0	N/A	93.0	9.59×10^{-6}	N/A	N/A	N/A	N/A
			81.0	1.59×10^{-6}	86.0	1.06×10^{-4}	84.0	1.27×10^{-4}
III	87.1	$<10^{-12}$	93.5	1.43×10^{-4}	N/A	N/A	N/A	N/A
IV	N/A	$<10^{-12}$	86.9	3.78×10^{-5}	N/A	N/A	N/A	N/A
V	N/A	$<10^{-12}$	87.5	8.78×10^{-5}	N/A	N/A	N/A	N/A
VI	N/A	N/A	102.0	N/A	N/A	N/A	N/A	N/A

Fracture surfaces of the neat epoxy and the nanocomposite were compared using SEM. The nanocomposite has 0.5 wt% of functionalized MWCNTs and has been fabricated following Process VI. Figures 9(a) and 9(b) are low-magnification fracture surfaces of the neat epoxy and the nanocomposite, respectively. The surface roughness increases with MWCNT content. The high-magnification micrograph of Fig. 9(c) indicates a good bonding between MWCNTs and the matrix.

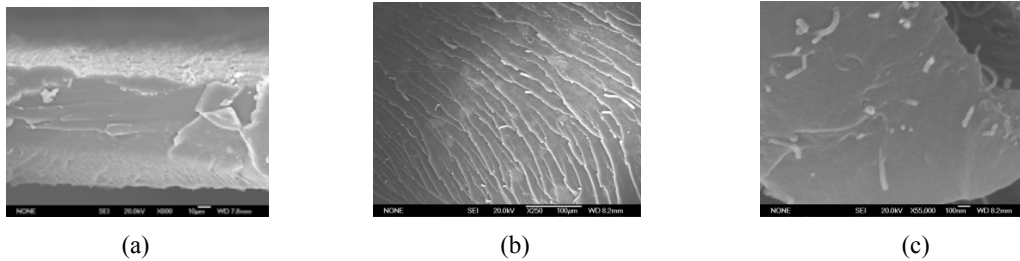


Fig. 9. SEM micrographs of fractured surfaces: (a) neat resin, (b) MWCNT-IL(PF₆)/epoxy (0.5 wt%) nanocomposite at low magnification, and (c) MWCNT-IL9Cl/epoxy (0.5 wt%) at high magnification.

3.3.3. MWCNT-IL(Cl)/epoxy composite

The same Process VI was used to fabricate MWCNT-IL(Cl)/epoxy composites with only one exception. That is, the solvent used was a mixture of ethanol and acetone. At 0.5 wt%, this composite is seen to be slightly stronger than the one based on PF₆ ionic liquid, Table 2. Also, the nanocomposite shows a percolation threshold (lower than 0.1 wt %) that is lower than typical CNTs/epoxy composites (around 0.5 to 0.6 wt %). The highest DC conductivity is 8.38×10^{-3} S/cm with 1 wt% of MWCNTs. This value is almost the highest conductivity we can find on CNT/epoxy composites.

Table 2. Properties of MWCNT-IL(Cl)/epoxy composite

	Tensile strength(MPa)		Conductivity (S/cm)
Neat	85		$<10^{-12}$
0.1%	98	99	1.05×10^{-4}
0.2%	103	105	7.65×10^{-3}
0.5%	109	108	8.16×10^{-3}
1%	106		8.38×10^{-3}

As with the MWCNT-IL(PF₆)/epoxy composite, the MWCNT-IL(Cl)/epoxy composite also shows good dispersion and good bonding between MWCNTs and the epoxy, Fig. 10. Most nanotubes are seen to be broken rather than just having been pulled out of the matrix.

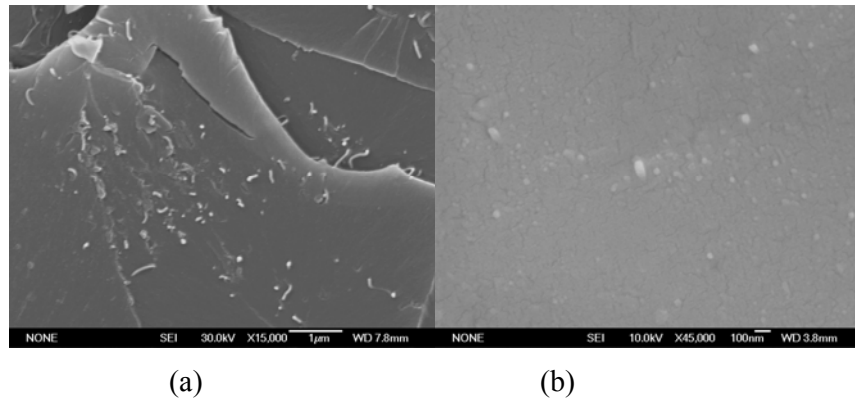


Fig. 10. SEM micrographs of fractured surface of MWCNT-IL(Cl)/epoxy (0.5 wt%) nanocomposite: (a) low magnification and (b) high magnification.

3.3.4. Preparation of hierarchical thin film composite

An optimum process has been established after 5 process variations have been tried to produce void-free composite. In order to save material, only one layer of carbon fiber fabric was used. The optimized process steps are as follows:

- (1) Mix curing agent and Epon, stir and degas in vacuum oven for 30-40 min.
- (2) Pour into a preheated mold, immerse the fabric into epoxy and degas in vacuum oven for 20-30

min.

(3) Cover with an aluminum lid wetted with Epon and shake the mold.

(4) Degas in vacuum oven for 20-30 min and cure at 120°C 4 h.



Mold



Tensile specimen



Conductivity specimen

Fig. 11. Fabrication mold and test samples.

Photographs of an aluminum mold, a tensile specimen and a conductivity specimen are shown in Fig. 11. Table 3 summarized the properties of CF/epoxy composites with and without MWCNTs. As the fiber volume fraction was not kept constant, the measured properties were normalized with respect to the fiber volume fraction. These normalized values are shown together with the measured values. The tensile strength does not change much as MWCNTs are introduced, as expected. However, the normalized conductivity almost doubles with the addition of MWCNTs. The results are yet preliminary, and more extensive results will be provided in the future.

Table 3. Preliminary properties of hierarchical carbon fiber/epoxy composites

Composite	Fiber volume %	Tensile strength (MPa)		Conductivity (S/cm)	
		Measured	Normalized	Measured	Normalized
CF/Epoxy	28	362	1293	2.65	9.46
CF-CNT/Epoxy	13	136	1046	2.26	17.38

Appendix A

Contents

Fig. A-1. SEM image of a bare Carbon Fiber (CF).	16
Fig. A-2. Change of the surface on the carbon fiber fabric with various catalyst film thickness and temperature for 10 min under 160 sccm Ar gas and 40 sccm C ₂ H ₂ gas.	17
Fig. A-3. Change of the surface on the carbon fiber fabric with various catalyst film thickness and time at 850 °C under 160 sccm Ar gas and 40 sccm C ₂ H ₂ gas with Ni catalyst depositions.	18
Fig. A-4. Change of the surface of the carbon fiber fabric after thermal CVD at 850 °C for 90 min under 185 sccm Ar gas and 15 sccm H ₂ gas with xylene and ferrocene. The flow rate was (a) 0.195 ml/hr and (b) 1.95 ml/hr.	19
Fig. A-5. STEM EDS analysis of the CF specimen after thermal CVD at 850 °C for 90 min under 185 sccm Ar gas and 15 sccm H ₂ gas with xylene and ferrocene after 10 nm Ni catalyst deposition.	20
Fig. A-6. Change of the surface on the carbon fiber fabric with various catalyst film thickness and time under 2000 W irradiation power.	21
Fig. A-7. Morphology of the surface on a carbon fiber with Ni catalysts after microwave irradiation. The irradiation power was (a) 400 W, (b) 800 W, (c) 1200 W, and (d) 2000 W.	22
Fig. A-8. STEM EDS analysis of the CF specimen after Microwave Irradiation System at 2000 W for 40 sec under 180 sccm Ar gas and 20 sccm H ₂ gas with Ni catalyst deposition.	23

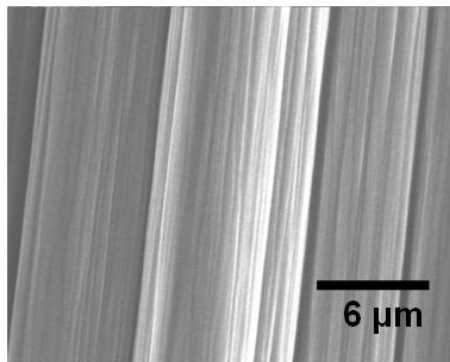


Fig. A-1. SEM image of a bare Carbon Fiber (CF).

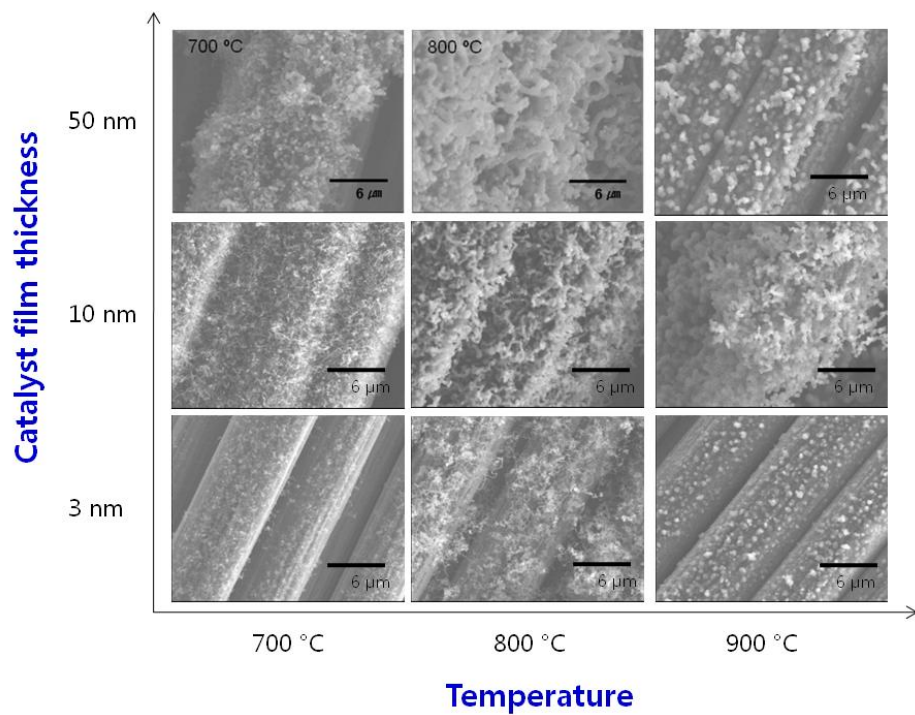


Fig. A-2. Change of the surface on the carbon fiber fabric with various catalyst film thickness and temperature for 10 min under 160 sccm Ar gas and 40 sccm C₂H₂ gas.

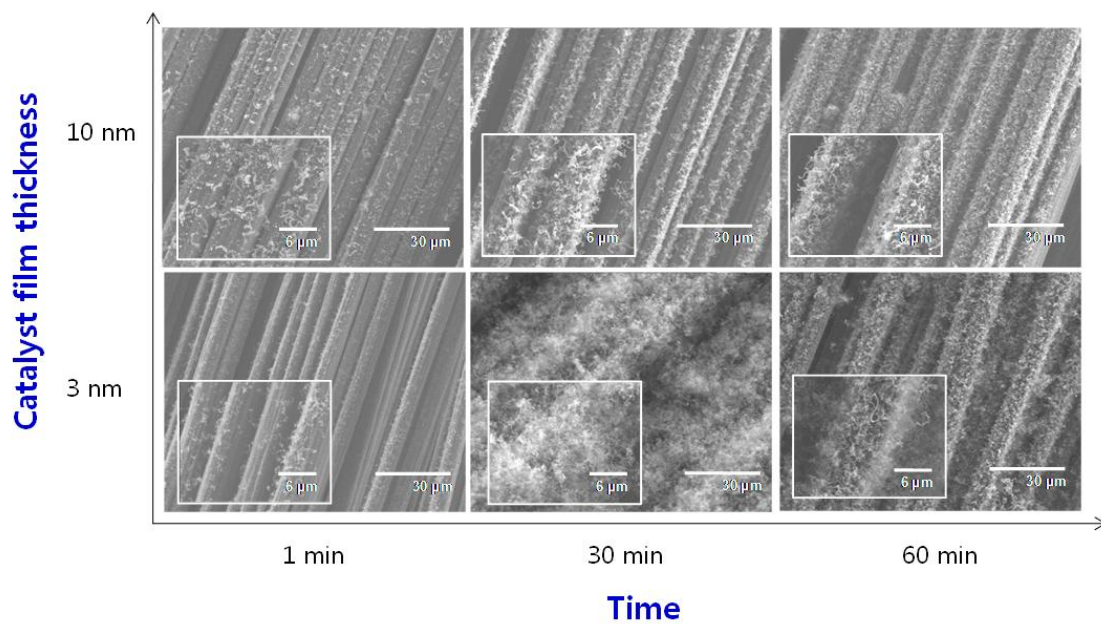
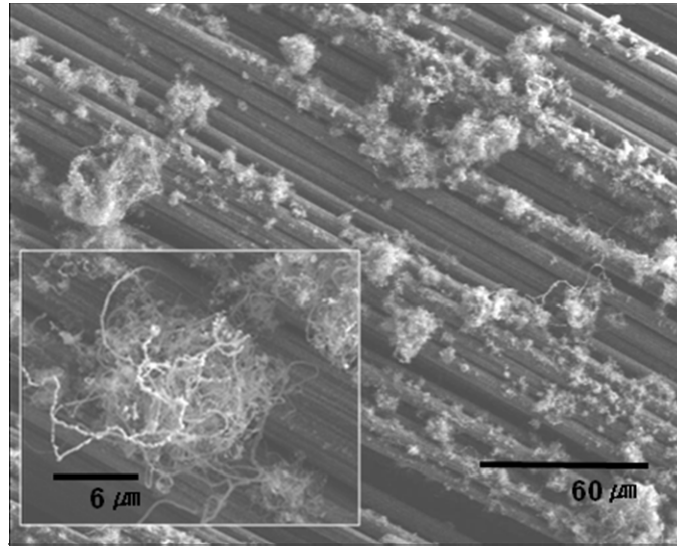
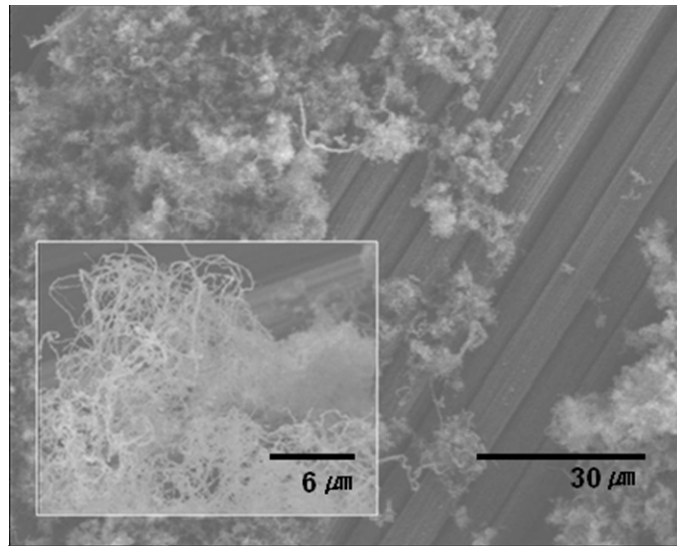


Fig. A-3. Change of the surface on the carbon fiber fabric with various catalyst film thickness and time at 850 °C under 160 sccm Ar gas and 40 sccm C₂H₂ gas with Ni catalyst depositions.



(a)



(b)

Fig. A-4. Change of the surface of the carbon fiber fabric after thermal CVD at 850 °C for 90 min under 185 sccm Ar gas and 15 sccm H₂ gas with xylene and ferrocene. The flow rate was (a) 0.195 ml/hr and (b) 1.95 ml/hr.

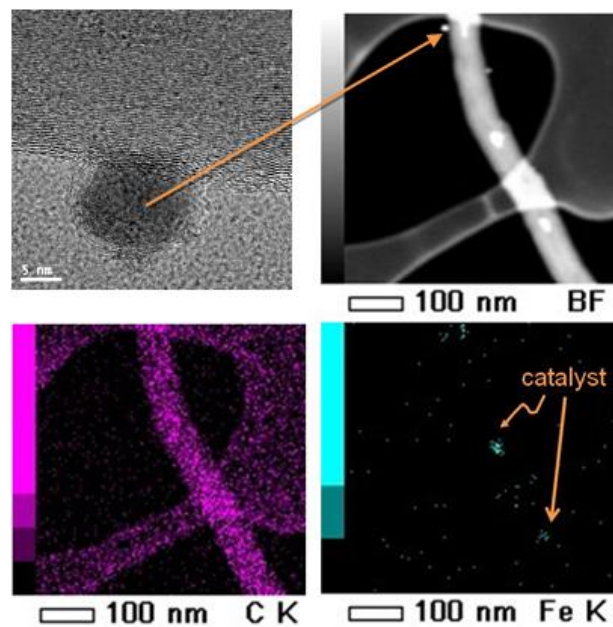


Fig. A-5. STEM EDS analysis of the CF specimen after thermal CVD at 850 °C for 90 min under 185 sccm Ar gas and 15 sccm H₂ gas with xylene and ferrocene after 10 nm Ni catalyst deposition.

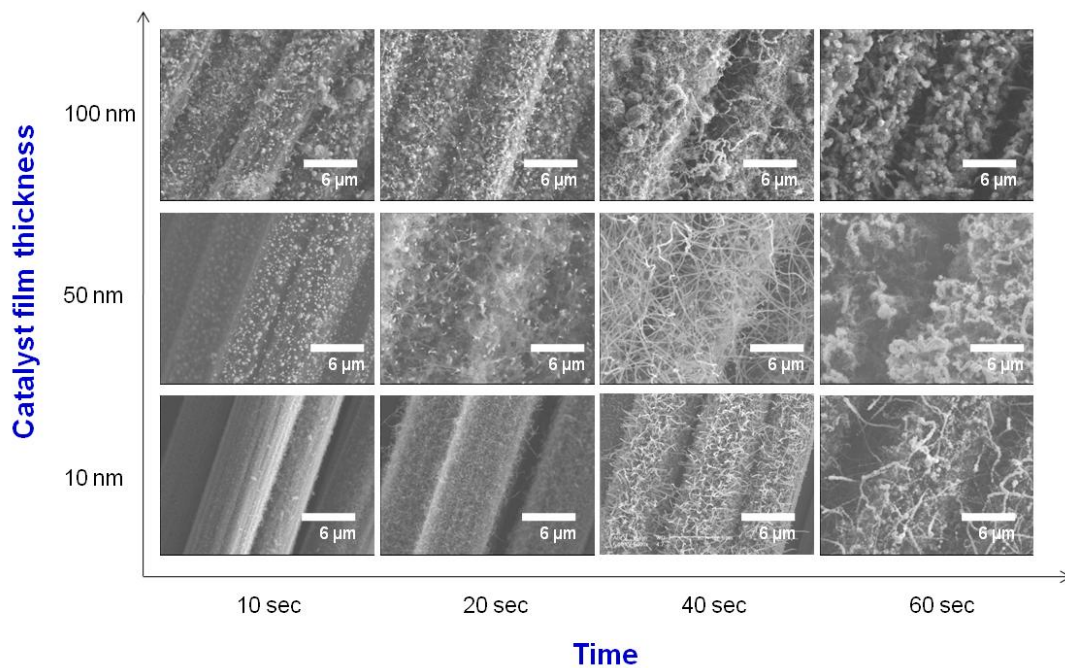


Fig. A-6. Change of the surface on the carbon fiber fabric with various catalyst film thickness and time under 2000 W irradiation power.

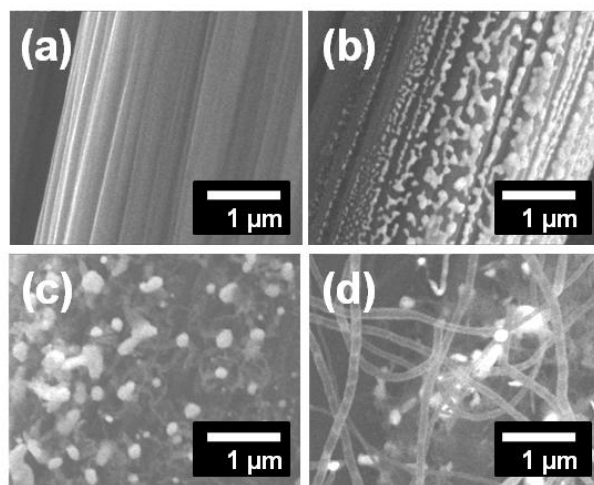


Fig. A-7. Morphology of the surface on a carbon fiber with Ni catalysts after microwave irradiation. The irradiation power was (a) 400 W, (b) 800 W, (c) 1200 W, and (d) 2000 W.

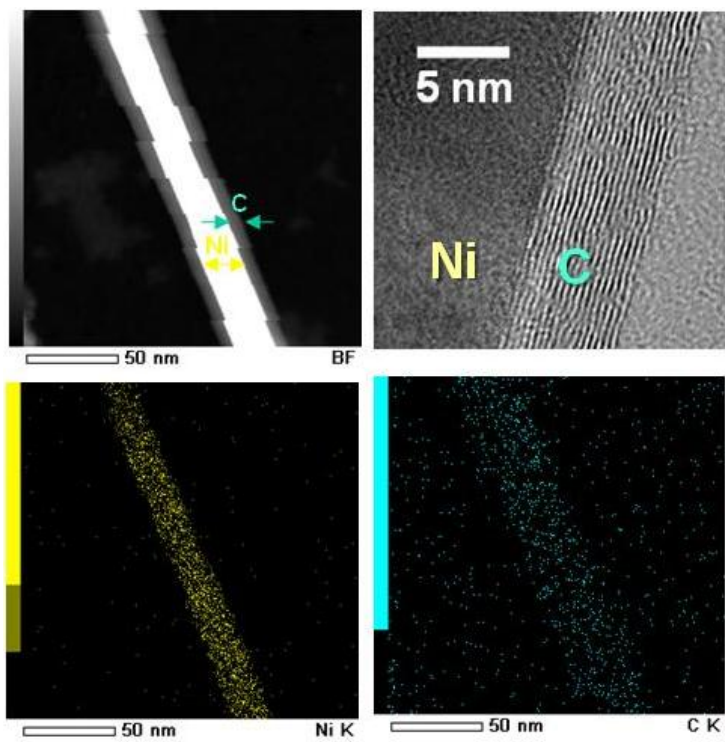


Fig. A-8. STEM EDS analysis of the CF specimen after Microwave Irradiation System at 2000 W for 40 sec under 180 sccm Ar gas and 20 sccm H₂ gas with Ni catalyst deposition.

The Final Report

Title: Distributed Detection of Attacks/Intrusions and Prevention of Resource-Starvation Attacks in Mobile Ad Hoc Network

Principal Investigator:

Professor Jong Kim, Pohang University of Science and Technology
(CSE)

Telephone: +82-54-279-2257

Facsimile: +82-54-279-2299

E-mail: jkim@postech.ac.kr

Contract Number: FA4869-07-1-4069

AOARD Reference Number: AOARD-074069

AOARD Program Manager: Sang-ho Byun

Period of Performance: 1 year

Submission Date: 8 Oct 2008

NBIT Program 2008

Final Report

Project Title

Distributed Detection of Attacks/Intrusions and Prevention of Resource-
Starvation Attacks in Mobile Ad Hoc Network

2008-10-06

Korean Principal Investigator (KPI)		US Principal Investigator (USPI)	
Full Name	Jong Kim	Full Name	Kang G. Shin
Affiliation (department)	Pohang University of Science and Technology (CSE)	Affiliation (department)	The University of Michigan (EECS)
Position	Professor	Position	Kevin & Nancy O'Connor Professor
Telephone	+82-54-279-2257	Telephone	+1-734-763-0391
Fax	+82-54-279-2299	Fax	+1-734-763-8094
E-mail	jkim@postech.ac.kr	E-mail	kgshin@eecs.umich.edu

A. Project Goal (of Korean Research Group)

The main purpose of this research is to address the problems of detecting malicious/compromised nodes and preventing resource-starvation attacks in mobile ad hoc networks (MANETs). Related to our purposes, we have 3 research items (objectives) as follows:

- Item 1 : Reliable and efficient detection of malicious nodes
- Item 2 : Prevention of energy consumption attack
- Item 3 : Selfish router detection in wireless mesh networks

B. Progress report

1 Item 1 : Reliable and efficient detection of malicious nodes

1.1 Introduction

To increase the network lifetime of MANETs, we proposed the Distributed Energy Efficient Cluster Formation (DEECF) scheme which exploits the expected residual energy of mobile nodes to determine the cluster head and starts the cluster formation from the node with having one neighbor (leaf node) to reduce the number of stand-alone (solitary) cluster. The expected residual energy is the energy of mobile nodes considering both the current remaining energy level and the energy consumption rate of a node. We have conducted extensive experiments using the ns-2 simulation tool to validate the DEECF scheme.

1.2 Clustering Algorithm

The DEECF scheme is composed of two steps, the information exchange step and the cluster formation step. In the information exchange step, each node exchanges its own information, which consists of the node ID, the state, the expected residual energy, and the number of neighbors. Then, in the cluster formation step, each node decides its own role as cluster head or cluster member from the information received from its neighbors.

1.2.1 Information exchange step

In this step, nodes exchange information between neighbors. Initially, every node knows only its own information and is classified as unspecified node. Each node broadcasts HELLO packet with the information, such as ID and the state, to identify its neighbors. Then, each node calculates its own expected residual energy. After calculating the expected residual energy, each node broadcasts SEND_INFO packet with its own information such as ID, the expected residual energy, and the number of neighbors.

1.2.2 Cluster formation step

This step forms clusters using the information, such as node ID, state, the expected residual energy, and the number of neighbors, received from neighbors of each node. At first, each node compares the degree and ID with unspecified neighbors and decides whether to have a chance to be the cluster head primarily. The node with the smallest degree among

unspecified neighbors has the chance to be the cluster head. If there is more than one node with the smallest degree among unspecified neighbors, the node with the largest ID among them has the chance to be the cluster head. The reason is that there may be a network without leaf nodes. In such a case, head selection cannot be performed if there is no deciding rule based on the node ID. The node with the chance to be the cluster head compares the expected residual energy with unspecified neighbors and decides whether to be the cluster head. If the node has the most expected residual energy among unspecified neighbors, the node changes the state into CLUSTER_HEAD and broadcasts HEAD_DECLARATION message to neighbors. Otherwise, the node passes the chance to an unspecified neighbor node with the most expected residual energy.

1.3 Simulation results

We compared the DEECF scheme with the distributed energy priority cluster formation (DEPCF) scheme [1] and the distributed degree priority cluster formation (DDPCF) scheme [2], in terms of the network lifetime and the number of cluster heads. The DEPCF scheme chooses the node having the most current residual energy as the cluster head. The DDPCF scheme selects the node having the highest degree as the cluster head.

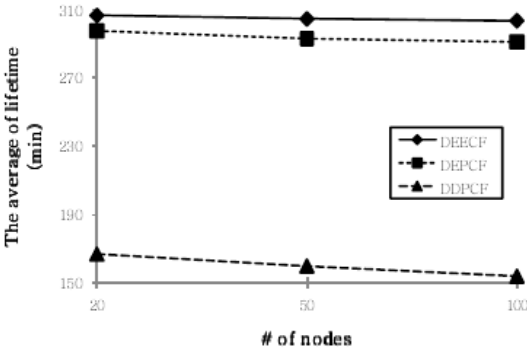


Fig. 1 The average of the network lifetime

Figure 1 shows the mean of the network lifetime according to the increase of the number of nodes in the network when the initial energy of every node and the energy consumption rate for detection are set to 30 kW and 2.0, respectively. Figure 1 shows that the DEECF scheme has longer network lifetime than the DEPCF and DDPCF schemes by 4 % and 47.5 % in the average case, respectively. This is because the cluster heads in the DDPCF scheme, which are assigned due to the largest degree, are changed only when there is a topology change while the cluster heads in the DEECF scheme and the DEPCF scheme are changed in every cluster reconstruction time due to the change in the residual energy.

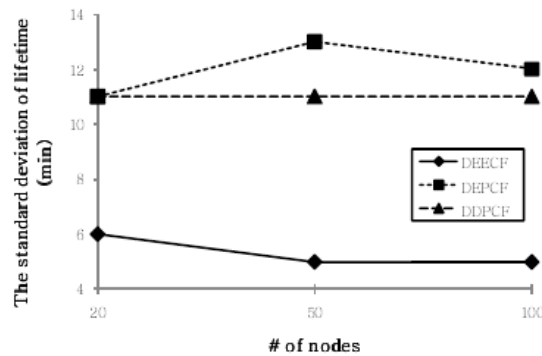


Fig. 2 The standard deviation of the network lifetime

Figure 2 shows the standard deviation of the network lifetime. In all cases, the standard deviation of the network lifetime of the DEECF scheme is less than that of other two schemes. It means that the DEECF scheme is the most stable in the various topologies.

2 Item 2 : Prevention of energy consumption attack

2.1 Introduction

MANET has no infrastructure and each node must play special roles like being a router. Thus, availability of each mobile node can be target of security attacks. Especially, as mobile nodes usually have limited battery power, the energy consumption attack to exhaust power of nodes is one of main issues in the field of MANET security. With the energy consumption attack, a malicious node can make other nodes tortured with power trouble.

In this research, we focus out the energy consumption attack in the transport/application layer. As a new type of the energy consumption attack in the transport/application, we introduce the *steady-slow attack*, which is a new type of energy consumption attack which we refined through this research. Also we discuss about prevention approaches which annuls the energy consumption attack effectively.

2.2 Steady-slow Attack

Because mobile nodes are dependent on battery power, it is important to minimize their energy consumption. The energy consumption by the network interface is significantly high, especially for smaller devices.

Turning the devices to low-power states when they are not in use is an important technique to conserve energy for battery-powered wireless devices. The IEEE 802.11 power saving mode is one of the most popular techniques in wireless LAN and multi-hop wireless networks to coordinate the power states of communication devices [3]. Approximately 50% of energy saving can be achieved using the IEEE 802.11 PSM in multi-hop wireless networks [4].

Steady-slow attack is a new type of energy consumption attack which disturbs the mobile device in low-power states without excessive packet forwarding. Usually power saving technique such as IEEE 802.11 PSM is used in conjunction with time-out driven policy. Steady-slow attack makes mobile devices to keep high-power states by exploiting this characteristic.

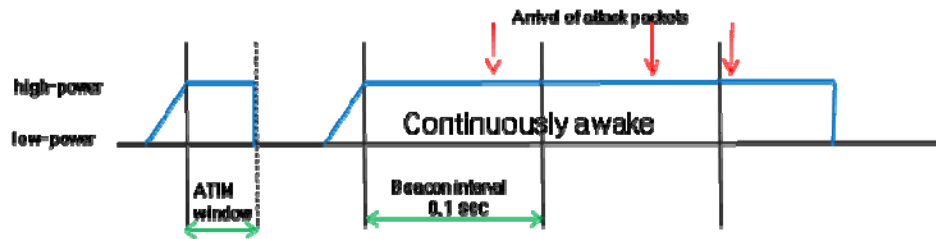


Fig. 3 Steady-slow attack

2.3 Approaches for Preventing energy consumption in the Transport/Application Layer

In previous works, they mainly focused on the energy consumption attack in MAC layer or simple flooding attack in the network layer. To deal with the consumption attack, they proposed authentication-based solutions or simple rate-limiting-based solutions. However these solutions are not proper to prevent not-excessive attack, such as the *steady-slow attack* since they are based on rate-limiting concept and designed for MAC or network layer. In our research, we are studying about destination-dominating defense scheme against energy consumption attack, allowing intermediate nodes and a destination node to suppress effect of the consumption attack. The reason why we consider a destination node dominating scheme is the resilience against transport/application layer consumption attacks relies on end-to-end detection mechanisms. In other words, intermediate nodes in MANET are difficult to decide whether certain packets are malicious or not in the transport/application later.

Our scheme basically consists of three steps:

- i. Attack recognition/detection at a destination node
- ii. Attack notification to the network
- iii. Reaction at intermediate nodes

Basically we think that it is not difficult for a destination node to determine where sequential incoming packets are meaningless or malicious to him. If the attack is detected at a destination node, the node profiles the malicious packets and generates filtering rules to enable mobile nodes to filter out those malicious packets. And then, the destination propagates the rules into the network. Now the intermediated nodes can react against the energy consumption attack.

3 Item 3 : Selfish router detection in wireless mesh networks

3.1 Introduction

In Wireless Mesh Networks, Mesh Routers (MRs) should be cooperative to communicate each other. However, selfish MR can exist to conserve own bandwidth by dropping other nodes' packets. Such selfish behavior in routing causes serious damage such as packet delivery ratio decrease and latency increase to other nodes. Moreover, it gives continuous damage due to location-interdependency between MRs [5]. To solve the selfish behavior problem in routing, most of previous researches [6, 7] rely on network monitoring. However,

network monitoring causes too much overhead to the router in real networks because a router should deal all the packets passing it. According to our experiments, when the tcpdump [8] tool is being executed, it causes 10~20% performance decrease in networking. For this reason, we propose a novel technique for detecting a selfish router. Our scheme detects a selfish router using application-level packet delivery tests. We expect that our scheme detects a selfish router with low overhead and high accuracy.

3.2 Selfish Router Detection with Packet Delivery Test

Packet delivery test is to check whether an intermediate router between two routers adopts a selfish routing policy or not. If a router drops a test packet following a selfish routing policy, packet delivery test will fail. Then the proposed scheme picks it as a selfish router. The proposed scheme consists of three phases.

3.2.1 Preparation phase

In preparation phase, an agent collects routing tables from MRs and finds optimized pairs of routers, satisfying following,

- Maximize the # of MRs to be covered by test
- Minimize the # of max overlapped MR
- Minimize the # of max overlapped link

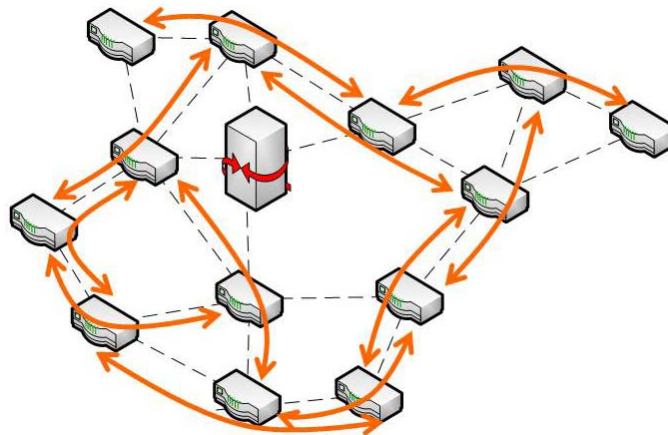


Fig. 4 An example of pair selection

Figure 4 shows an example of pair selection. Central node presents a server, and other nodes are MRs. Both ends of arrows are test pair, and intermediate MR of them is a node to be tested.

3.2.2 Packet delivery test phase

After preparation step, an agent in a server commands a test start. Then each pair starts a

packet delivery test.

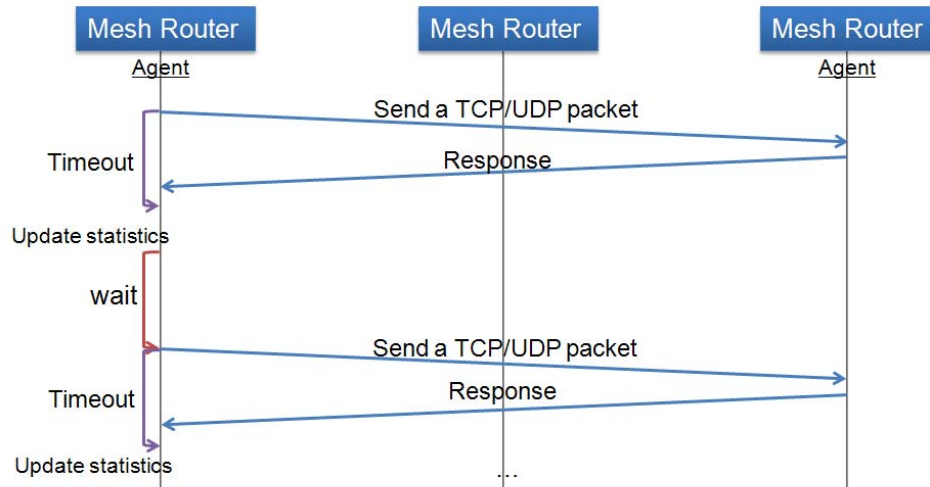


Fig. 5 Packet Delivery Test flow

Figure 5 shows a packet delivery test flow. Left-side and right-side MR present test routers and the middle MR presents a router being tested. One MR of a test pair sends a packet, then the other replies for the packet. If an intermediate MR drops a test packet for pursuing own selfishness, then test will failed. Otherwise, the test will succeed. According to the test statistics, the proposed scheme detects a selfish router.

3.2.3 Punishment phase

If a selfish MR is detected, it should be punished to discourage selfishness. Most of the previous related works punished a selfish MR with isolation. We have studied how to punish a selfish MR, but we think that punishment in our scheme will also be based on isolation because isolation is the most powerful motivation to suppress the selfishness and to encourage cooperation in routing.

C. Summary

As above mentioned, we are currently handling 3 research items. For item 1, we proposed the clustering algorithm for cluster-based IDS in MANETs, which is named as the Distributed Energy Efficient Cluster Formation (DEECF) scheme. In order to increase the network lifetime, the DEECF scheme uses the expected residual energy to determine the cluster head and starts the cluster formation from the leaf nodes to reduce the number of clusters. Simulation results show that the DEECF scheme provides a longer network lifetime than the DEPCF and the DDPCF scheme.

For item 2, as one of energy consumption attacks in the transport/application layer, we introduced the *steady-slow* attack, which cannot be covered by defense approaches of previous work. To cope with this type of energy consumption attack, we are studying about destination-dominating defense scheme, allowing intermediate nodes and a destination node

to suppress effect of the consumption attack. This work is still under a scheme-design process.

For item 3, we addressed a selfish routing problem in WMNs. We have studied the seriousness of selfish routing in WMNs and related works. To deal with selfish behavior in routing, previous works adopt network behavior monitoring which causes too much overhead in a real network. We proposed the selfish router detection scheme using application-level packet delivery tests. This method is expected to reduce overhead in detecting a selfish router. Embodying the procedure is under progress.

Reference

1. Wu, J., Gao, M., and Stojmenovic, I. On calculating power-aware connected dominating sets for efficient routing in ad hoc wireless networks. *IEEE/KICS Journal of Communications and Networks* 4 (2002), 59–70.
2. Xin, J., Yao-Xue, Z., Yue-Zhi, Z., and Yaya, W. A novel ids agent distributing protocol for manets. *Lecture Notes in Computer Science* 3515 (May 2005), 502–509.
3. R. Zheng, J. Hou and L. Sha, Performance analysis of IEEE 802.11 power saving mode, in: *Proceedings Communication Networks and Distributed Systems Modeling and Simulation Conference (CNDS)* (2004).
4. R. Zheng and R. Kravets. On-demand power management for ad hoc network. In *Proceedings of the The 22nd Annual Joint Conference of the IEEE Computer and Communications Societies (INFOCOM)*, 2003.
5. L. Santhanam, B. Xie, D. P. Agrawal, “Selfishness in Mesh Networks: Wired Multihop MANETs,” in *IEEE Wireless Communication Magazine*, 2008.
6. S. Marti, T. J. Giuli, K. Lai, and M. Baker, “Mitigating routing misbehavior in mobile ad hoc networks,” in *Proceedings MobiCom 2000*, 2000, pp. 255–265.
7. L. Santhanam, N. Nandiraju, Y. Yoo, and D. P. Agrawal, “Distributed self-policing architecture for fostering node cooperation in wireless mesh networks,” in *Proceedings of the PWC*, Vol. 4217, pp. 147-158, 2006.
8. <http://www.tcpcdump.org/>